Mediating the Liquid Chromatography Wall Effects using Diamagnetic Repulsion

By

Nathan Camilleri

Department of Chemistry and Biomolecular Sciences

Macquarie University

This Thesis is submitted in fulfilment of the requirements for the degree of

Masters of Research (MRes)

9th of October 2015

Performed under the supervision of

Dr. Christopher R. McRae

Table of Contents

Declaration of Originality

I declare that the work presented in this thesis has been carried out by myself and has not been submitted in part or in full to any other university or institution for any other reward.

Nathan Camilleri

October 2015

Acknowledgements

There have been a number of people over the span of this project that have helped me, offered advice or generally been a pleasure to work under the same department with. However, I'd like to reserve these acknowledgements for those who have had the greatest impact during the span of my MRes.

My first and greatest thanks has to go to my supervisor Chris. You have been the most prevalent influence on me as a chemist throughout both my undergraduate and postgraduate education. Your dedication to your students is incredible, with such a personal investment of yourself to our development as chemical researchers. Thank you for the privilege of working under your supervision for my MRes and for giving me the odd nudge in the right direction for my research.

My second thanks goes to Gin who has self-assigned herself as my second mother, dictating what food I cannot eat (the amazingly delicious 'Real Australian Beef Noodles') and what music I'm not allowed to listen to (the kings of hip-hop Tupac and Biggie). In all seriousness though, you have not only been a wonderful friend but also a remarkable research colleague. I don't think I could ever separate my memories of MRes from your cheerful company, bad jokes and embarrassing dancing.

I also have to thank Ben, who like Gin and I, has also completed his MRes this year. Although we weren't in the same research group, I always felt our discussions about each other's research was beneficial (probably more to me – doubt I was very helpful with organic synthesis). Thanks for listening to my rants about how magnets have free will and offering useful suggestions throughout my MRes.

Thank you also to Raha, Anthony, Harry and Ryan for your support during the project.

Abbreviations and Acronyms

DCM	Dichloromethane
CNC	Computer Numerical Controlled
CTC	Carbon Tetrachloride
FEMM	Finite Element Method Magnetics
HETP	Height Equivalent to a Theoretical Plate
HPLC	High Performance Liquid Chromatography
ID	Internal Diameter
PEEK	Polyether Ether Ketone
UHPLC	Ultra-High Performance Liquid Chromatography

List of Tables

List of Figures

Abstract

The variation in packing density as a function of column radius has been demonstrated to be a major limitation in the efficiency of liquid chromatography columns. Referred to as the wall effects, these changes in bed structure across the diameter of the column cause the distortion of eluting solute profiles from flat discs to parabolic in shape. These parabolic profiles are measured as having a faster, more efficient migration in the column centre with a slower, less efficient migration at the column wall.

The possibility of using diamagnetic repulsion as an approach to mediate these effects was investigated using an on-column visualisation chromatography system. A series of magnetic fields were applied to various columns formats to determine if solute migration from the column wall could be achieved. A distinct migration of solute from the column walls was observed for small scale pipette columns indicating the principle of diagenetic repulsion may be a feasible approach. However, migration of iodine in both a 15 mm and 4.0 mm internal diameter (ID) column indicated no repulsion was achieved. Discrepancies between these results may have been a result of changed magnet array position relative to the chromatography column.

Chapter 1: Introduction

1.1 Preamble

Liquid chromatography, whilst being the most widely applied analytical technique, suffers from poor separating power compared to other chromatography techniques such as gas chromatography. Past approaches to increasing the separating power, also called the efficiency, of liquid chromatography columns have usually taken one of two forms; by increasing the physical length of the column or by decreasing the particle size of the stationary phase. Whilst effective, these approaches have severe limitations in terms of practicality. As a result, alternative strategies for improving column efficiency have attracted significant commercial and academic interest.

Packed chromatography columns have long been known to suffer efficiency losses due to what are referred to as the wall effects. In essence, the wall effects arise from inconsistencies in packing density occurring at the wall which distorts elution bands of a mixture's components, reducing column efficiency. Their considerable contribution to column inefficiency prompted the development of 'Active Flow Technology', a series of new column designs patented by ThermoScientific that mediate efficiency loss from the wall effects. Unfortunately, these new column designs require the purchasing of specialised fittings and additional pumping systems so are not directly translatable to standard High-Performance Liquid Chromatography (HPLC) systems.

The thesis presented investigates the possibility of an alternative method for mediating the wall effects that does not require any modification of the HPLC system. This proposed method exploits the diamagnetic properties of compounds to repel solute away from the walls of the column in an attempt to improve column efficiency. The application of magnetic fields to chromatography for this purpose is entirely novel and may offer significant advantages over the patented column designs of ThermoScientific.

1.2 Liquid Chromatography

1.2.1 Principles of Liquid Chromatography

Chromatography is a technique used in the separation of components in a mixture and can be coupled with numerous post separation detectors for their quantification or identification.

Separation using this technique is achieved through the competitive distribution of these components between two phases, one that is stationary and another that is mobile and moves in a definite direction. Compounds which have a higher affinity for the mobile phase will elute first, whilst compounds with a higher affinity for the stationary phase will be retained for longer periods. Specifically, liquid chromatography is defined as having a liquid mobile phase and typically employ a solid stationary phase, which may be modified with a hydrophobic or hydrophilic liquid.

1.2.2 Chromatography Efficiency

Since the purpose of chromatography is the physical separation of two or more components in a mixture, separating power is the primary parameter by which columns are judged. Columns with poor separation performance pose one of two problems to the chromatographer. If being used for preparative applications, the target component of the mixture being purified may be contaminated by other closely eluting components. For analytical purposes, where compounds are recorded as peaks by a post-column detector, peaks may overlap causing their area to no longer be proportional to concentration.

The separating power of a column is measured as a numerical value, called the efficiency, which is understood in terms of Plate Theory. This theory proposes that the separation processes in chromatography can be considered as a series of theoretical plates. At each of these plates, a partitioning equilibrium of the analyte exists between the mobile and stationary phases. The greater the number of plates, the greater the separating power. It is this quantity that efficiency measures.

The efficiency of a column is calculated through a consideration of peak widths and retention times measured by a post-column detector, shown in Equation 1.

$$\mathrm{N} = 5.545\left(\frac{\mathrm{t}_R}{\mathrm{w}_h}\right)^2 \text{ (Equation 1)}$$

Where **N** is the number of theoretical plates, $\mathbf{t_R}$ is the retention time of the peak and $\mathbf{w_h}$ is the peak width at half height. Once the number of plates has been calculated for a column of defined length, the height equivalent to a theoretical plate (HETP) can be determined using a simple expression, presented in Equation 2.

$$\mathrm{HETP} = \frac{\mathrm{L}}{\mathrm{N}} \text{ (Equation 2)}$$

Where **HETP** is the height equivalent to a theoretical plate and **L** is the length of the column. The HETP of a column is informative as it is related directly to the physical processes that contribute to peak broadening. This relationship is described by the van Deemter equation [1] presented in Equation 3.

$$\mathrm{HETP} = \mathrm{A} + \frac{\mathrm{B}}{\mathrm{v}} + \mathrm{Cv} \text{ (Equation 3)}$$

Where **v** is the velocity of the mobile phase and **A**, **B** and **C** are quantities representing the amount of broadening due to eddy diffusion, axial diffusion and resistance to mass transfer respectively. The reduction of any one of these quantities offers a means to improve the efficiency of a chromatographic separation.

1.2.3 Common Approaches for Improving Efficiency

To avoid separation problems such as co-elution and peak overlap, there are a number of common approaches available to the chromatographer for improving the efficiency of a column. However, these methods often come with some consequence. The most simple of these is to increase the physical length of the chromatography column. Assuming HETP is kept constant, the total efficiency of a column will increase proportionally with length, as given by Equation 2. This approach has the downside of increasing back pressure, analysis time and solvent consumption proportionally to the increase in length, meaning it is not suitable for routine or high through-put analysis.

Another common approach to increasing column efficiency is to decrease the particle size of the stationary phase. Smaller particles have provided considerable gains in efficiency for chromatography columns, with particles now reaching sub-2 µm [2]. However with smaller particle size, higher pressures are required to push mobile phase through the column packing necessitating the use of ultra-high pressure pumping systems. This has given birth to a new generation of liquid chromatography termed Ultra-High Performance Chromatography (UHPLC) which has unfortunately found use primarily in niche applications due to its additional cost investments.

1.3 The Wall Effects

1.3.1 Background

The notion of a ‘wall effect’ in chromatography systems can be attributed to the early works of Knox et al. [3,4] who studied columns dry packed with 21 µm diameter particles. The conclusion from these studies was that the stationary phase in packed columns was radially heterogeneous which was detrimental to their performance. They proposed that the column bedding was comprised of two sections; a central circular core containing a random bed and an outer region

whose structure is dictated by the requirements of the columns smooth cylindrical wall [3]. This radial heterogeneity of column packing alone contributes up to 70% of the eddy dispersion constant (A) in the van Deemter equation (Equation 2) [5], having detrimental consequences for column efficiency. With this complication realised, the effects of the wall on separation have been the focus of research for over 40 years. During this time, several distinct wall effects have been identified and their nature extensively studied.

1.3.2 The Geometric Wall Effect

The first of these effects is the geometrical wall effect which arises from the geometry of the spherical particles and a smooth column wall. As these particles can only touch the wall but not penetrate it, a close packing configuration cannot be achieved at the immediate vicinity of the wall [6,7]. Additionally, particles packed against the wall form a more ordered conformation with a higher void fraction compared to the random packing of the column core [8,9]. As a consequence, permeability of the column packing is at its highest within a few particle diameters of the wall which results in higher mobile phase velocity [10,11]. This enhanced flow results in solute eluting faster at the walls compared to the rest of the column. Consequently, the flow profiles of solutes are distorted, leading to peak fronting and lower column efficiency particularly for narrow column formats.

1.3.3 The Frictional Wall Effect

The frictional wall effect is a product of slurry packing procedures used for preparing chromatographic columns, primarily those used for analytical purposes. As the name implies, this wall effect arises from the friction generated during the packing process. In slurry packing the stationary phase is compressed under a high flow-rate pushing solvent or compression piston in order to consolidate the bed and prevent any movement or shuffling of the stationary phase [12]. The high pressures used for consolidation result in a build-up of stress between particles in contact with one another. Frictional forces prevent particles from sliding or rolling against each other, resulting in this stress being translated particle to particle until it is directed against the column wall [13]. As more compression is applied, particles are forced harder and harder against the column wall. Ultimately, this leads to an increase in the packing density occurring at the outer regions of the column near the wall [6,8,14]. In contrast to the geometrical wall effect, the frictional wall effect results in a lower void fraction occurring near the wall, reducing its permeability [15,16]. This systematically reduces mobile phase velocity and distorts solute profiles from flat disks to a parabolic shape

resembling that of a partially filled bowl [6,7]. As a consequence, each component elutes from the column over a longer period of time, contributing to peak broadness, tailing and column inefficiency.

1.3.4 Other Wall Effects

The geometric and frictional wall effects are those commonly associated with particle packed chromatography columns. However, there are a number of other wall effects that are prevalent in other column types. For instance, dry packed particle columns are subject to wall effects very different to those that are slurry packed. During the dry packing of columns, a segregation of particles occurs, with larger and coarser particles occupying the region closest to the walls [17]. This has the opposite consequences to the frictional wall effect, with higher permeability and mobile phase velocity occurring near the wall [18].

Other wall effects are also observed in monolithic columns which, opposed to employing individual particles, contain a porous silica rod stationary phase formed through the polycondensation of silanes. As this reaction is exothermal and takes place inside the column, temperature gradients are generated, with higher temperatures in the column core [19]. The reaction then proceeds faster in the column core, producing a radially heterogeneous monolith [20]. As a consequence, a more permeable wall region is created resulting peak tailing as measured by a detector [21].

1.4 Approaches for Investigating the Wall Effects

1.4.1 End column detection

End column detection techniques were the first to be used for investigating radial heterogeneity in column beds. The first example of its use were on columns that were prepared using dry packed 21 µm diameter particles [4]. At the end of the packing material, electrodes were placed at specific radial locations to observe the differences in efficiency for packing near the wall and at the centre of the column. The study found that mobile phase velocity increased as the wall was approached [3], consistent with our understanding of the dry packing wall effect. This increase in velocity was also accompanied by increases in HETP from 1.7 at the column centre, to 4.7 within 1 mm of the wall [4]. Agreement was found with later studies that used microelectrodes on commercially prepared slurry packed columns, with HETP measured as substantially higher at the wall [22,23]. However, as the columns were prepared using a slurry packing method, the mobile phase

velocity decreased as the wall was approached with a 5% greater retention time for solute measured near the wall [22].

End column detection was further developed by using a fluorescent detector combined with optical fibers to increase the spatial resolution of the technique [17,24,25]. In general agreement with previous studies, velocities were systematically slower near the column wall with a difference of up to 13% for a preparative and 10% for an analytical column compared to the column centre [25]. However, one important difference was observed. Mobile phase velocity was measured as being slightly higher within a few particle diameters of the wall [17], providing the first evidence of the geometrical wall effect.

1.4.2 Nuclear Magnetic Resonance

End column detection methods had the disadvantage of only observing effects post chromatography column. In response to this limitation, NMR techniques were developed to visualise solute migration and mobile phase flow taking place inside the chromatography column [26,27]. Imaging of the solute bands showed trailing at the column walls, distorting the band from a flat disk to that of a partially filled bowl. Higher resolution NMR techniques were also applied to investigate flow inhomogeneity as a function of column radius as well as axial distance for columns packed using different methods [28]. The results of a dry packed and slurry packed column are shown in Figure 1.

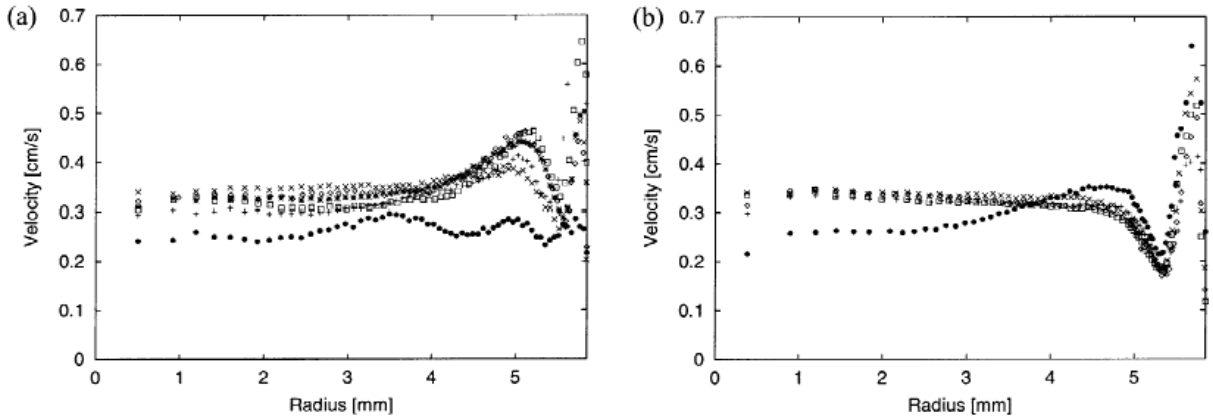

Figure 1: Plots of axial mobile phase velocity as a function of column radius for columns packed with impermeable 99 µm diameter polystyrene beads using (a) the dry packing method and (b) the slurry packing method. Data was collected from a number of distances from the entrance distributer: •= 1 mm; + = 4 mm; □ = 7 mm; * = 10 mm; × = 13 mm [28].

Common between the columns was that the highest mobile phase flow was observed within 5 particle diameters of the wall as a result of the geometric wall effect [28]. However, opposite flow trends were observed for the dry and slurry packed columns in the region near the wall. The column

prepared using a dry packing method (Figure 1 (a)) showed increases in mobile phase flow velocity as the wall was approached, maximising approximately 1 mm from its surface. The opposite trend was observed for slurry packed columns (Figure 1 (b)) where axial flow velocity was shown to decrease as the wall was approached, consistent with the frictional wall effect.

1.4.3 Matched Refractive Index

Matched refractive index techniques have also been developed for on-column visualisation, offering even greater resolution capabilities. With its origins in the earliest work investigating wall effects [4], the matched refractive index approach was developed further to allow quantitative visualisation of solute profiles [29,30]. In this method, a transparent column is packed with stationary phase and has a mobile phase flow as per normal HPLC. However, the phases are selected such that their refractive indices are matched, eliminating the opaque nature of the column and making it appear transparent. A coloured species can then be applied to the column and its elution recorded using a high resolution photographic detector. Grayscale images can then be calibrated against standards of known concentration allowing the distribution of the analyte within the column to be calculated [30].

Matched refractive index techniques have been applied to slurry packed columns, providing distinctive images of the geometrical and frictional wall effects distortion of flow profiles [6]. With a localised injection of iodine near the column wall (Figure 2 (a)), the slower mobile phase flow near the wall causes the circular solute profile to becomes diagonally distorted as a function of elution time. Conversely, with an injection at the wall (Figure 2 (b)), increased mobile phase flow at the immediate wall vicinity causes a spike to protrude from the solute profile nearest the wall.

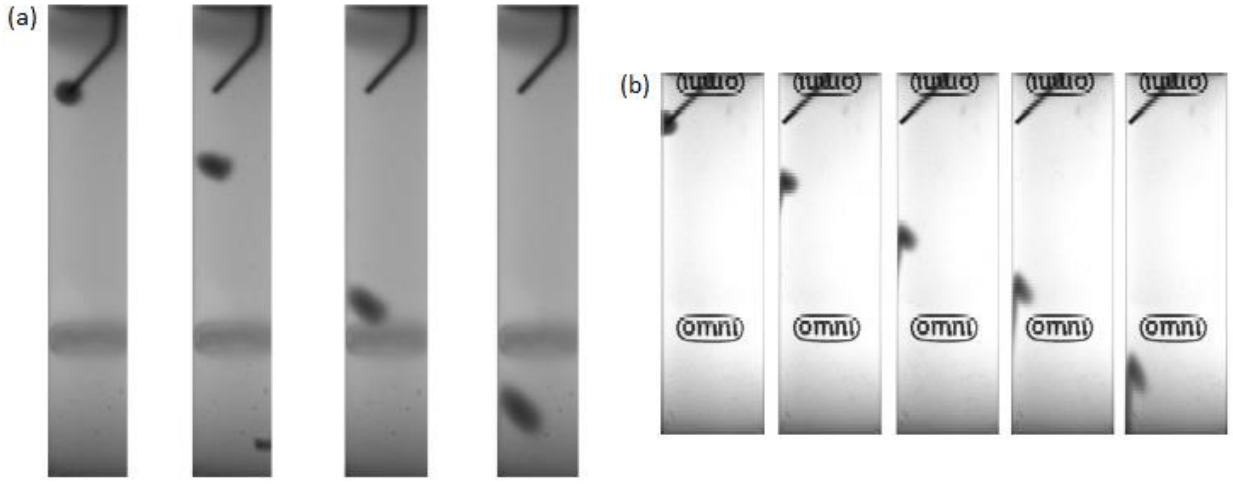

Figure 2: Photographs of a 10 µL injection of iodine migrating along a chromatography column in which the mobile and stationary phases have matched refractive indices. The injection was made at (a) 0.6 × r (column radius) and (b) at the column wall [6].

1.4.4 Confocal Laser Spectroscopy

Confocal laser spectroscopy has been another successful approach used to achieve on-column visualisation. As opposed to measuring migration of the analyte or mobile phase, this technique characterises the internal stationary phase structure. Originally developed for determining the macropore morphology of silica monoliths [31-33], confocal laser spectroscopy has also found its applications in analysing the three-dimensional bed structure of particle packed capillaries [9,34,35]. Reconstruction of column internal structures from the spectroscopic data has shown significant fluctuations in packing porosity as a function of radius, illustrated in Figure 3.

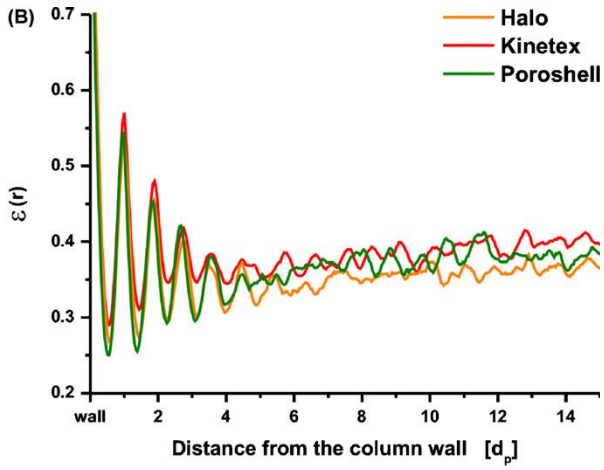

Figure 3: Radial porosity profile of capillaries packed with core shell particles, covering a distance from the capillary wall into the bulk structure of the bed [9].

The highest porosity of the column is at the very wall surface. This is caused by the spherical stationary phase only being able to touch, but not penetrate the column wall. At one particle radius from the wall, porosity is at its lowest before increasing to another maximum at one particle diameter's distance. The porosity of the bed oscillates in this fashion, with decreasing amplitude, toward the column centre within 5 particle diameters of the wall. Beyond this distance, the wall can no longer impose an ordered structure on the bed and porosity reaches that of the column bulk with low-level random fluctuations. The porosity of the packing is the most important contributor to the permeability of the column packing and translates to the velocity biases of the geometric wall effect [9].

1.5 Active Flow Technology

1.5.1 Design

To address the efficiency losses caused by the wall effects, ThermoScientific in partnership with the University of Western Sydney developed a novel column design which was subsequently patented in 2012 [36]. The new concept has been termed 'Active Flow Technology' and works by removing the wall portion of flow from the central portion before measurement by standard bulk detectors. Active flow technology has demonstrated significant improvements in column efficiency and incorporates two new column designs: parallel segmented flow columns [37] and curtain flow

columns [38]. The basis of these designs is shown in Figure 4, which consists of a frit where the inner portion is separated from the outer portion by a solid polyether ether ketone (PEEK) ring. The frit is contained in a special fitting consisting of a central port for the inner porous frit and three peripheral ports for the outer porous frit.

In the parallel segmented flow column design, the fitting shown in Figure 4 is employed at the outlet of the column. The sample is applied to the column as in standard HPLC, but only flow from the central port is collected for quantification. Flow from the peripheral ports are typically discarded but can passed through other detectors to allow multiplexed detection. Essentially what is created within the column is a 'virtual' column which is effectively wall-less, as the stationary phase used for the separation is not in contact with the physical column wall [7].

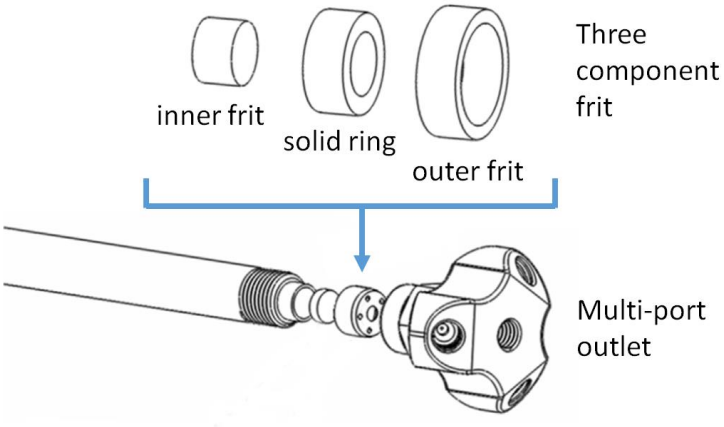

Figure 4: Illustration of a parallel segmented flow fitting showing the central port and three peripheral ports. The figure also illustrates the frit design, where the inner portion of the frit is separated from the outer portion by a solid PEEK ring [37].

The second column design of active flow technology is the curtain flow column which uses the same column fitting shown in Figure 4 except at both the inlet and outlet head. This design works using the principle of the infinite diameter column where solute does not come into contact with the column walls [3]. To achieve this, the sample is applied to the radial central portion of the column through the inlet central port. At the inlet peripheral ports, a curtain flow of mobile phase is passed, restricting analyte migration to the core of the column [38].

1.5.2 Efficiency Gains

Both active flow technology column designs have demonstrated considerable reductions in HETP. A study of a 4.6 mm parallel segmented flow column packed with 5 µm C18 media showed separation efficiencies 25-30% greater than the standard 4.6 mm column for a mixture of toluene, propylbenzene and butylbenzene [39]. Similar results were obtained for a study that compared both active flow management designs to equivalent standard columns. HETP was reduced by 15-31% and 27-41% for parallel segmented flow and curtain flow columns respectively [40]. Larger gains in

efficiency were observed for compounds with strong retention. Additionally, curtain flow designs were able to provide sensitivity gains between 2 and 3 fold [41].

1.5.3 Disadvantages

Active flow technology, while providing significant improvements in column efficiency, does have numerous disadvantages. The first of these is that the technology is not directly translatable to standard HPLC systems and obliges extra investment. To be used, the specialised proprietary fittings shown in Figure 4 must be purchased from ThermoScientific and an additional pumping system for use in curtain flow applications. Because of this, much like UHPLC columns, active flow technology may only find application in niche analyses.

Operating requirements may also be problematic for its routine application. Due to curtain flows design of having two distinct flows through the column, the solvent delivery systems for each must be matched so pressure pulsations from the pumps are synchronous [41]. When pumping devices are not matched, increases in system noise are observed [7], increasing limits of detection and quantification for analyses. This requirement adds another level of complexity for the HPLC operator. Finally, active flow technology is not suitable for preparative purposes because the outer portion of flow, and hence product, is discarded.

1.6 Diamagnetic Repulsion

1.6.1 Theory

All substances possess magnetic properties and are affected in some way by the application of a magnetic field. Substances that are attracted to magnetic fields are referred to as paramagnetic, whereas those that experience repulsion are classified as diamagnetic. To be classified as paramagnetic, a compound must have a non-zero spin or orbital angular momentum, which arises from the presence of unpaired electrons [42]. In these cases, the substance produces a flux in the same direction as an applied magnetic field and will experience a force towards regions of highest field strength [43]. Unlike paramagnetism, diamagnetism is a property of all electrons whether paired or unpaired [42]. Diamagnetic substances experience repulsion in magnetic fields by producing a flux in the opposite direction to the applied field, moving from regions of high field strength to regions of lower strength [43]. The overall magnetic property of a compound is calculated from its total paramagnetic and diamagnetic contributions. This property is measured as a magnetic

susceptibility, which is positive for paramagnetic substances and negative for diamagnetic substances [42].

1.6.2 Current Applications

A number of studies have been published in the literature that highlight diamagnetic properties as a means of repulsive substance manipulation. Earlier examples of its application can be seen in the development of systems to separate diamagnetic particles according to their magnetic susceptibilities using inhomogeneous magnetic fields [44-48]. This type of technique, termed magnetophoresis, has been used for the label free separation of cells [44,45] and polymer particles suspended in paramagnetic solution [46,47]. Diamagnetic repulsion has also been applied as a means to trap particles along capillaries [48,49]. In these studies, two rare earth neodymium magnets were placed either side of a capillary with opposite poles facing one another. This orientation creates a region of high magnetic flux at a point along the capillary whose intensity decays rapidly along the axis of the capillary. As diamagnetic particles approach the region of high field intensity, they are repelled and will not pass between the magnets.

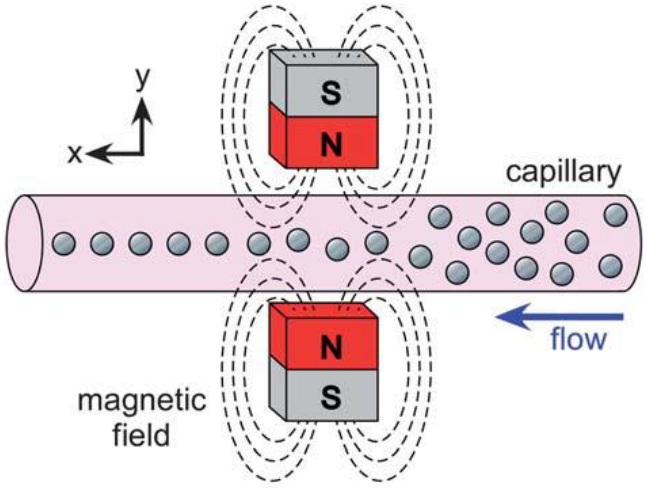

Figure 5: Principle of the flow focusing effect using diamagnetic repulsion. Diamagnetic particles enter the capillary distributed across its entire width. As they pass between the magnets they are repelled toward the centre of the capillary [50].

More relevant to this research, diamagnetic repulsion has also been used for the flow focusing of particles suspended in a paramagnetic solution [48,50]. A 150 µm capillary was placed between two neodymium magnets 0.7 mm apart with like poles facing one another [48,50]. As magnetic field lines cannot cross, this arrangement creates an area of zero magnetic field in the centre of the capillary. The effect of the magnetic field on the flow of diamagnetic particles is shown in Figure 5. Upstream to the magnet pair, diamagnetic particles were distributed over the entire width of the capillary. After passing through the pair of magnets, the particles were focussed into a narrow stream ±20 µm at the capillary centre [48].

1.6.3 Application of Diamagnetic Repulsion as a means to mediate wall effects

The application of magnetic fields to mediate the chromatography wall effects is a novel concept not yet explored in the literature. It shares the same principle as the flow focusing experiments discussed previously; to direct compounds away from the walls of a tubular container to improve the quality of an analysis. Hence, a similar approach will be used to investigate whether the same aims can be achieved. Specifically, a high magnetic field will be produced at the walls of the chromatography column with a magnetic minimum occurring at the centre axis. In theory, diamagnetic molecules will then experience a force away from the column walls and be focused in the column centre. Consequently, diamagnetic solutes will not be subjected to the chromatography wall effects and improvements in separation efficiency may result.

1.7 Project Aims

The work of this project can be broken down into three distinct aims. These aims are as follows:

1. Perform a proof of principle experiment to verify diamagnetic repulsion has to potential to manipulate solute migration in chromatography columns.
2. Develop a liquid chromatography system that allows the on-column visualisation of solute migration.
3. Quantify the effect of various magnetic environments on solute migration in a chromatography column.

Chapter 2: Experimental

2.1 Chemicals

Dichloromethane (DCM) (Lab-Scan, pestiscan grade) and methanol (Fronine Laboratory Supplies, reagent grade) were used without any additional purification. The stationary phase for pipette scale columns was 40 Å, 70-230 mesh silica gel (Sigma Aldrich, high purity grade). Stationary phase for 15 mm and 4.0 mm ID columns was 60 Å, 15-40 µm silica gel (Merck, chromatographic grade). All stationary phases were activated at 120 °C for at least 24 hours before use. Iodine (BDH Chemicals) was purified by sublimation. Glycerol (BDH Chemicals) was dried under vacuum at 60 °C for at least 48 hours before use. Carbon tetrachloride (CTC) (Sigma Aldrich, HPLC grade) was initially used without further purification. Due to CTC's adverse environmental effects and discontinued commercial availability, all CTC was recycled after use. Recycling procedure was as follows. Dissolved iodine was reduced using a sodium thiosulfate (BDH Chemicals) and water solution. Water layer was decanted and CTC purified by fractional distillation. Distilled CTC was then dried using 4 Å molecular sieves (Sigma Aldrich) which had previously been activated at 450 °C for 24 hours.

2.2 Small Scale Pipette Columns

The bottom of a soda glass Pasteur pipette was stoppered with cotton wool and packed using a 50% (v/v) slurry of 60 Å, 70-230 mesh silica gel in DCM. The column bed was packed to a height of 7 cm and a 1 mm layer of calcinated sand was evenly added to the top of the silica. The DCM mobile phase was lowered to the level of the silica packing and a volume of 20 g L^{-1} iodine in DCM solute was loaded to the radial centre of the column. See respective figures for the volume of the injection. DCM mobile phase was introduced carefully to the centre of the column so not to disturb the column bed or introduce a bias to the elution of the iodine band. Elution was repeated on the column in the absence of presence of magnetic fields.

2.3 Magnetic Simulations

Magnetic simulations were performed using Finite Element Method Magnetics (FEMM) software (D. C. Meeker, Finite Element Method Magnetics, Version 4.2, http://www.femm.info). N52 grade neodymium magnets were simulated with dimensions of 10 mm × 10 mm with air as the surrounding medium.

2.4 Measurement of Magnetic Field Strength

Magnetic field strength was measured using a DC Gaussmeter Model GM1-ST manufactured by AlphaLab Inc.

2.5 Chromatographic System

The chromatography system consisted of a GBC LC 1150 HPLC Pump connected to an Alltech Select Degassing System. Chromatography columns were secured within a Perspex viewing cell filled with dry glycerol. A 4000 K fluorescent light and two light dispersers were placed behind the viewing cell. Solute imaging was achieved using a Samsung EK-GC200 digital camera. Digital camera parameters were as follows for all solute migration analysis; 1/100 second shutter speed, F5.0 aperture, 100 ISO (sensitivity), 4000 K colour temperature and multipoint metering. The fluorescent light, viewing cell and digital camera were all mounted to a metal rig to ensure no movement of any components during or between analyses.

2.6 Solute Migration in a 15 mm ID column

A 15 mm ID borosilicate column was equipped with a fixed length outlet fitting and adjustable inlet fitting. Both the inlet and outlet fitting housed a 10 µm PTFE frit. The chromatography column was slurry packed in a downward configuration using a 40% (v/v) slurry of 60 Å, 15-40 µm silica gel in methanol. The packed bed was consolidated using a methanol pushing solvent at 20 mL min^{-1} for 15 minutes. The adjustable column inlet was lowered to axially compress the silica bed by approximately 3 mm. The final bed height was approximately 8 cm. The column was then secured and submerged in a viewing cell containing dried glycerol.

Runs were performed using a 100% CTC mobile phase at 1.5 mL min^{-1}. A background image of the column was taken with the photographic detector prior to injection. A 50 µL volume of 12 g L^{-1} iodine in CTC was then injected and used as the solute for band visualisation. Images were collected in 30 second intervals until the solute reached the column outlet. Injections were performed in duplicate without the application of magnets and in the presence of a rotating conformation magnet array.

2.7 Solute Migration in a 4.0 mm ID column

A 100 mm × 4.0 mm ID borosilicate column was equipped with two fixed length fittings for the column outlet and inlet. Both the inlet and outlet fitting housed a 2 µm steel frit. The chromatography column was slurry packed in a downward configuration using a 40% (v/v) slurry of 60 Å, 15-40 um silica gel in methanol. The packed bed was consolidated using a methanol pushing solvent at 5 mL min^{-1} for 15 minutes. The column was allowed to settle for 24 hours before further consolidation using a methanol pushing solvent at 5 mL min^{-1} for 15 minutes. The column was then secured and submerged in a viewing cell containing dried glycerol.

Two separate conditions were used for solute migration analysis of the 4.0 mm ID column. The first used a 100% CTC mobile phase at 0.4 mL min^{-1} and an injection of 10 µL volume of 12 g L^{-1} iodine in CTC as the solute for band visualisation. The second used a 100% DCM mobile phase at 0.4 mL min^{-1} and an injection of 10 µL volume of 12 g L^{-1} iodine in DCM as the solute. A background image was collected prior to sample injection and images collected in 15 second intervals after injection until the solute reached the column outlet. Injections were performed in triplicate without the application of magnets and in the presence of alternating, repeating and rotating conformation magnet arrays.

2.8 Data Analysis

Data analysis was performing using ImageJ software (Rasband, W.S., Image J, Version 1.46r, U.S. National Institutes of Health, Bethesda, Maryland, USA, http://imagej.nih.gov/ij/, 1997-2014). Solute images and their respective background were converted to 8-bit grayscale and the “difference” operation performed between the two. The resulting image was rotated to correct for the angle of the chromatography column and cropped to the width of the column and length of the solute band. Cropped images were then converted to a text image where each pixel is represented as a grayscale number in a spreadsheet. Data processing of the text image was performed using Microsoft Excel 2013.

Chapter 3: Results and Discussion

3.1 Proof of Principle

As the application of magnetic fields to push solute away from the column wall during liquid chromatography is a novel concept, a proof of principle experiment was performed in order to demonstrate whether it had the potential of being used. To do this, small scale silica columns were prepared using a DCM mobile phase and run in the absence or presence of magnetic fields. Once prepared, an iodine and DCM solution was loaded to the top of the column at its radial centre. This was performed with some difficulty, as loading needed to be performed quick enough to prevent drying and cracking of the bed, but not too fast as to disturb the top silica layer of the bed. Either of these damages to the bed would result in distorted solute profiles and make it difficult to evaluate the effects of the magnetic field on solute migration. It also resulted in column life being short (between 1 and 2 runs) meaning replicates on the same bed were not always possible.

Initial magnetic fields were applied using a curved neodymium magnet with both a north and south pole on each face. The iodine sample was loaded at the top of the column bed in the absence of the magnet, with the band becoming exposed to the magnetic field after the initiation of mobile phase flow. The elution of the iodine solute is presented in Figure 6. Images are presented in their inverted colours to aid visualisation of the solute band, with white, blue and black indicating regions of high, low and zero iodine concentrations respectively. The axial streaks seen in the images are the results of reflections of external light and not a property of the solute band.

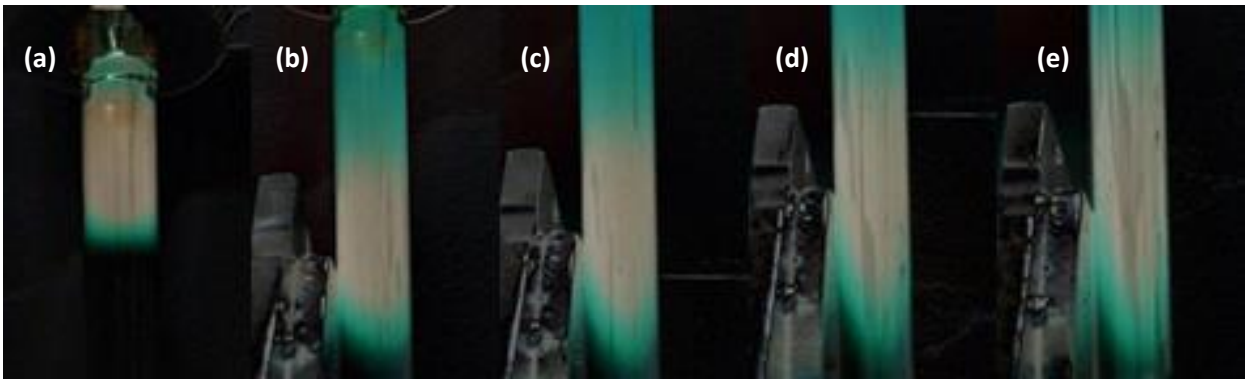

Figure 6: Elution of 200 µL of 20 g L^{-1} iodine in DCM through a small scale silica column with a curved neodymium magnet moved alongside the solute band on the left-hand side. Solute profiles were obtained by subtracting a background image and inverting the colour of images recorded at (a) 0, (b) 20, (c) 40, (d) 60 and (e) 80 seconds.

At time zero, the solute is seen to occupy either side of the column evenly. After mobile phase flow is initiated and the magnet positioned, a distinct migration of the solute from the surface

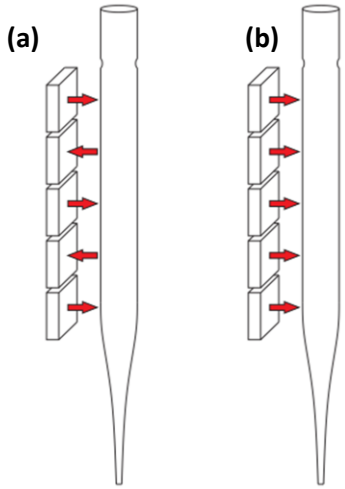

Figure 7: Different magnetic environments created using 10 mm × 10 mm × 3 mm neodymium magnets. Magnetised direction is indicated with red arrows. Magnet orientations illustrated are (a) alternating and (b) repeating.

of the magnet was observed. This effect is particularly clear at the front of the profile where the parabolic front is skewed toward the right. A distance is also created between the solute and the wall, which appears to become more pronounced with increased time in the magnetic field.

Solute migration however, was not always observed reproducibly. This may be the result of the relatively uncontrolled movement of the neodymium magnet which was positioned by free hand. To address this, stationary magnet arrays that spanned the length of the column were subsequently trailed. These arrays used 10 mm × 10 mm × 3 mm neodymium magnets in simple orientations illustrated in Figure 7. Trials using the alternating orientation (Figure 7 (a)) were unsuccessful in producing a visual migration of iodine walls of the column. However, greater success was achieved with the repeating conformation (Figure 7 (b)) which demonstrated a similar repulsion from the wall to that achieved using the curved neodymium magnet in Figure 6.

A packed pipette column was run in the presence of a repeating magnet array consisting of five 10 mm × 10 mm × 3 mm neodymium magnets followed by the absence of the magnetic field. This ensured that any change in solute profile observed in the presence of the magnet array was not caused by damaged sustained to the bed in a previous injection. The blank run is presented in Figure 8.

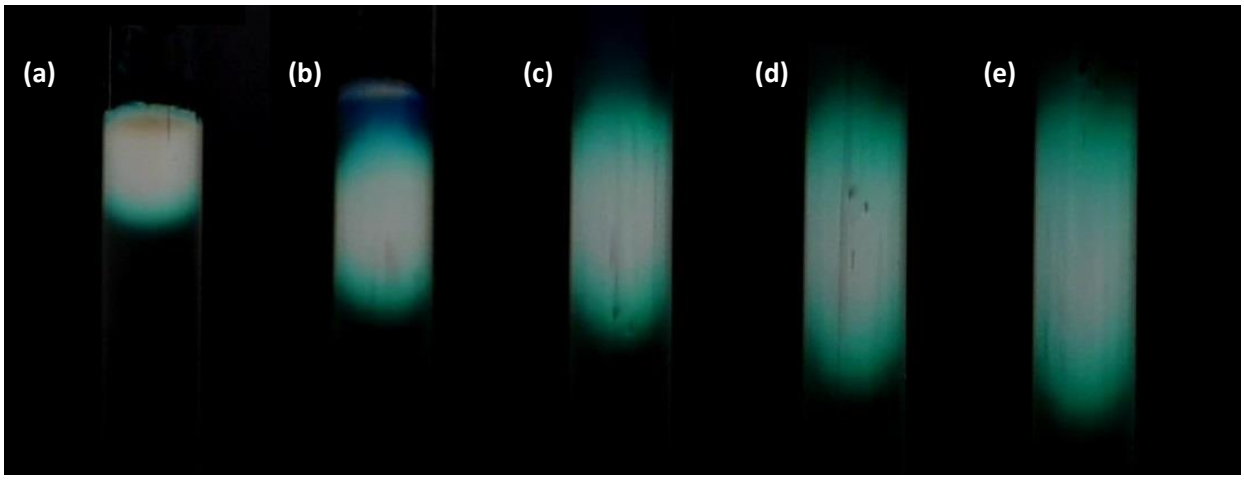

Figure 8: Elution of 100 µL of 20 g L^{-1} iodine in DCM through a small scale silica column. Solute profiles were obtained by subtracting a background image and inverting the colour of images recorded at (a) 0, (b) 20, (c) 40, (d) 60 and (e) 80 seconds.

At time zero, the solute is observed to be evenly distributed across the diameter of the column. Once mobile phase flow was initiated in the absence of a magnetic field, the parabolic front of the profile was enhanced and band broadening was observed to occur due to longitudinal and eddy diffusion. Most importantly however, the equal weighting of the iodine is maintained either side of the column for the duration of the elution.

The migration of the iodine solute in the presence the repeating magnet array is presented in Figure 9. Similar to the results with the moving neodymium magnet, a repulsion of the solute is observed within the first 20 seconds of elution. The parabolic front of the solute profile becomes increasingly skewed to the right with longer exposure to the magnet array (which is on the left). However the effect appeared to be less prominent in the axially central portion of iodine profile compared to that of the moving magnet. Where the moving magnet appeared to push the solute off the wall surface completely, the repeating conformation only showed a decrease in iodine concentration at the wall. This is indicated by the light blue colour occupying the space near the wall at 40 seconds and later compared to the blank run where the wall region appears whiter in colour.

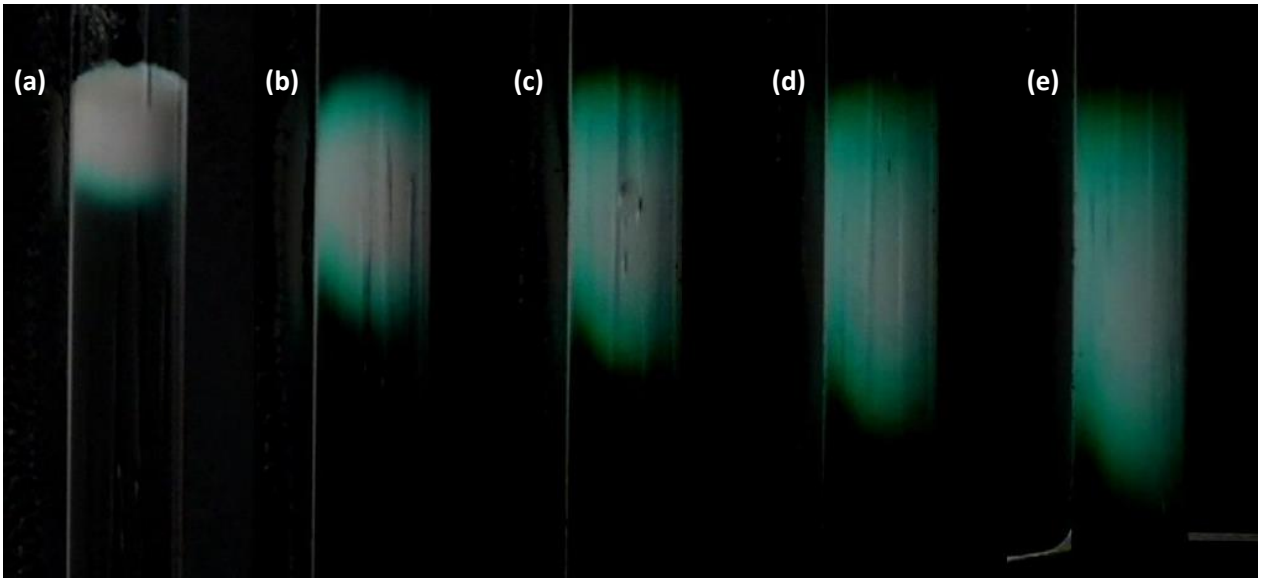

Figure 9: Elution of 100 μL of 20 g L^{-1} iodine in DCM through a small scale silica column with neodymium magnets in a repeating conformation positioned to the left-hand side. Solute profiles were obtained by subtracting a background image and inverting the colour of images recorded at (a) 0, (b) 20, (c) 40, (d) 60 and (e) 80 seconds.

Despite the used of stationary magnet arrays, issues with reproducibility still persisted. Magnet position was not precise relative to the column for replicate runs due to the crude nature of the experiments and may have contributed to this. The proof of concept experiment however did indicate a potential for diamagnetic repulsion to push solute from the column walls and hence may

offer an approach to mediate the wall effects. The experiments also stressed that precise positioning of magnets was crucial for reproducible success in repelling solute from the column walls. Further study was required to reproduce solute migration in a way that allowed quantitative analysis to determine the effectiveness of different magnetic environments at repelling solute from the walls.

3.2 Chromatographic System for On-Column Visualisation

3.2.1 Selection of methods

In order to quantify the effects of a magnetic field on solute migration, a chromatographic system that allows on-column visualisation was required. Three alternate approaches for on-column visualisation were described previously in Section 1.4. For the purpose of solute migration, confocal microscopy is not suited due to its limitation in only imaging the stationary phase structure. Similarly, NMR techniques are also not suited because they require the generation of strong magnetic fields. This would limit the control of the magnetic environment experienced by the column and is not compatible with the presence of permanent magnets. Therefore, the matched refractive index technique was selected. This technique allows imaging of solute migration at high resolutions and more importantly, is compatible with the application of magnetic fields to the chromatography column.

3.2.2 Development of the chromatographic system

The matched refractive index system works using the principles of the Beer-Lambert Law. That is, light from a source is passed through the sample and its transmission measured by a detector. Using this method, three distinct components must be addressed and optimised in the design of a system that provides accurate and reproducible analysis. These are the light source, the sample cell and the detector.

As visualisation of the migrating band is through transmission, the lighting conditions must be as uniform as possible. To achieve this, a 4000 K fluorescent light was selected as a neutral ‘white’ light source. The light was fitted with a diffuser and a second diffuser positioned between the light source and the column to ensure light was uniformly applied to the sample cell. Protection from interferences by external light was also implemented by using a cardboard barrier.

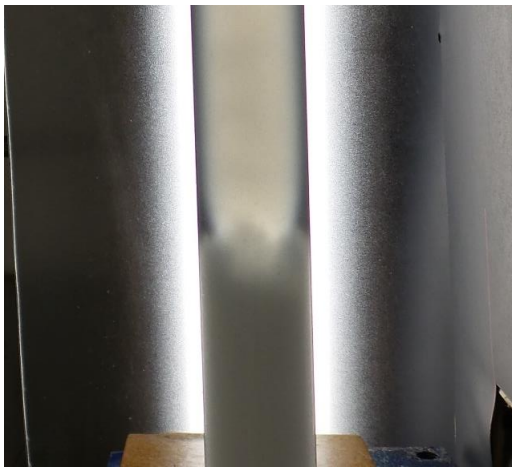

Figure 10: Solvent change from methanol (bottom) to carbon tetrachloride (top) in a column packed with a silica stationary phase.

The second component that must be considered is the column itself, which behaves as an absorption cell in photometry. The system must therefore permit the transmission of light through the column. The first issue that must be overcome is the material used to contain the stationary phase. This was addressed by using a borosilicate glass column which allowed the direct observation of the column packing. Secondly, the refractive indices of the stationary phase and mobile phase were matched to remove the opaque nature of the bed. Specifically, a silica stationary phase and CTC mobile phase were used, which had been reported in the literature as producing a transparent column [29]. The observations from this study were slightly different, with the column adopting a more translucent nature. This is illustrated in Figure 10, which shows the effect of replacing methanol with carbon tetrachloride in a column packed with a silica stationary phase.

The curvature of the glass column also has implications for the path which light travels from its source, through the column and to the detector. Under normal conditions, significant refraction of light would occur due to the columns cylindrical nature and differences in refractive indices between the column contents, column walls and the medium external to the column. This is referred to as the cylindrical lens effect [29] and distorts the inner dimensions of the column perceived by the detector. To limit this distortion, the column was submerged in a Perspex viewing cell containing dried glycerol. The refractive index of glycerol matches that of the borosilicate glass column [30], and significantly reduces the unwanted refraction of light. The effect of submerging the column in the glycerol viewing cell is shown in Figure 11. For the portion of the column not submerged in glycerol, the stationary phase appears to extend to the very edge of the column. The walls also appears darker due to the refraction of light away from the detector causing loss of information. However, once submerged,

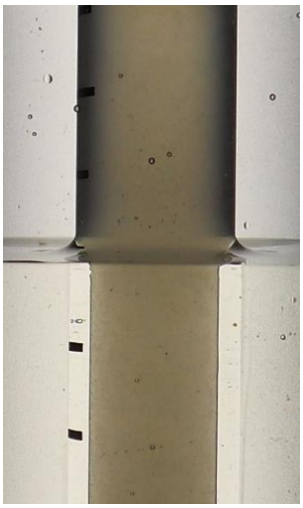

Figure 11: Image illustrating the cylindrical lens effect. Bottom portion of the column is submerged in glycerol and the upper portion remains surrounded by air.

the thickness of the column wall can be seen and the information lost at the column edge is negligible.

The final component of the system that must be considered is the detector. In this system, a high resolution digital camera was used as the detector, which had a number of parameters which affected the quality of the image collected. These were namely the shutter speed, aperture size and ISO sensitivity. Shutter speed was minimized to prevent blurring of the moving solute band whilst allowing enough light to reach the detector. Aperture size had a similar effect allowing the control of light allowed to reach the detector. A moderate aperture size was selected to compensate for the lower transmission of light through the translucent column bed. Finally the ISO sensitivity was minimised as higher settings resulted in considerable noise and are not recommended for high quality photography.

The light source, viewing cell and photographic detector were all secured to a metal rig to ensure no movement of the components occurred between or during analysis. The completed chromatography system is presented in Figure 12, indicating the location of each component.

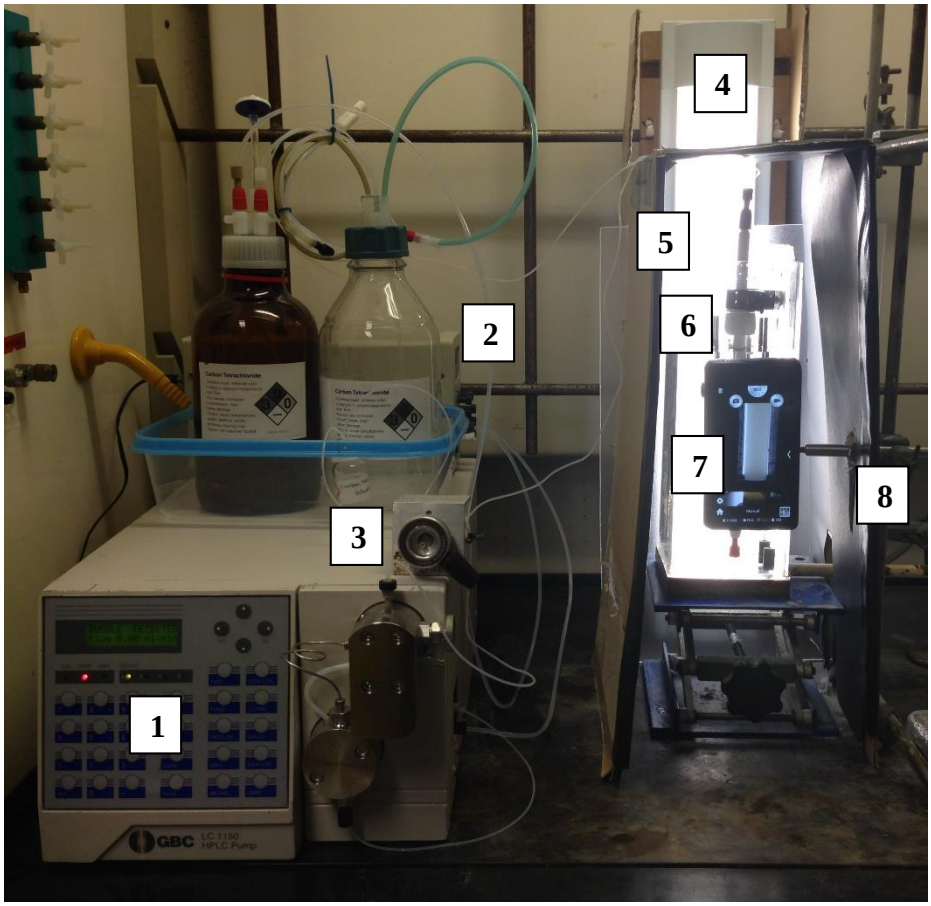

Figure 12: Chromatography system developed for on-column visualisation. Image shows (1) pump, (2) degasser, (3) injection port, (4) fluorescent light, (5), diffuser, (6) viewing cell containing column, (7) photographic detector and (8) camera mount.

3.2.3 Magnet Apparatus

As the proof of principle experiments demonstrated, slight positional changes in magnetic environments produced drastically different results for solute migration. Therefore, an apparatus that held the magnets in defined positions relative to the column was required. The apparatus had to also permit the transmission of light from the source, through the column and to the detector. The design of the apparatus is shown in Figure 13 and was constructed by the investigator from polyacetal plastic using a computer numerical controlled (CNC) mill.

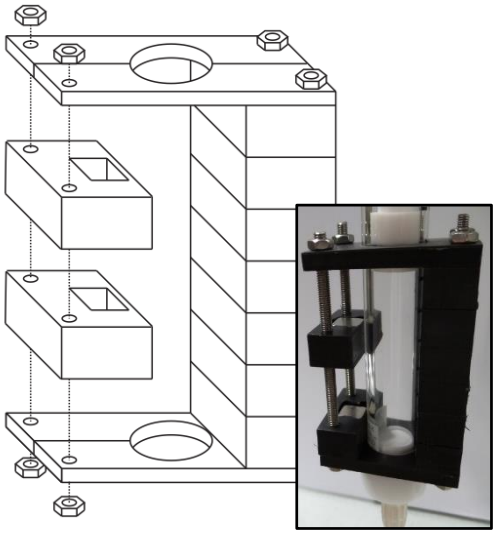

Figure 13: Constructed magnet apparatus developed for the precise positioning of magnets. Left hand side shows construction of the column with a hollow to house the magnets. Once loaded, a threaded rod can be inserted into the position as indicated by the dotted lines. The right hand side demonstrates an assembled column. The application of the apparatus to a column is demonstrated in inset.

The construction of the apparatus consisted of two columns to house the magnets to the left and right hand sides of the chromatography column. This allowed the magnets to be orientated in such a way that the field direction was perpendicular to the camera axis. The hollow of the apparatus was 10 mm × 10 mm to accommodate space for neodymium magnets with dimensions of 10 mm × 10 mm × 10 mm, allowing several magnetic orientations to be investigated using the single apparatus. Once loaded, the column is positioned in line with the centre of the magnet array. Also noteworthy is that the apparatus introduced an additional 1 mm distance between the magnets and the column.

3.3 Diamagnetic Calculations

3.3.1 Diamagnetic Repulsion Theory

As mentioned previously in section 1.5 of this thesis, diamagnetic molecules experience a force from regions of high magnetic flux towards regions of lower magnetic flux. The equation for the force experienced by a solid particle in a liquid medium is shown in Equation 4 [48].

$$F_{mag} = \frac{(X_p - X_m).V_p.B.(\nabla B)}{\mu_0} \quad \text{(Equation 4)}$$

Where $\mathbf{F_{mag}}$ is the magnetic force acting on a particle, $\mathbf{X_p}$ is the magnetic susceptibility of the particle, $\mathbf{X_m}$ is the magnetic susceptibility of the medium, $\mathbf{V_p}$ is the volume of the particle, **B** is

the magnetic flux density, $\mathbf{\nabla B}$ is the magnetic flux density gradient and $\boldsymbol{\mu_0}$ is the permeability of free space ($4\pi \times 10^{-7}$ H m^{-1}). This equation was derived for calculating the force experienced by polymer particles in a liquid medium, meaning the particle and the medium were in separate phases; one being a solid, and the other a liquid. Hence, any movement of the particle in one direction would require displacement of the liquid medium in the opposite direction to fill the space left behind. Hence, the magnetic susceptibility of the medium must be subtracted from that of the particle in the calculation of its magnetic force.

This scenario is not the case in a chromatography column. In chromatography the solute is in the same phase as the mobile phase and does not occupy space in the same way a solid does. The dissolution of a solute in a liquid is typically only accompanied by a minor increase in volume. Therefore, to an approximation, movement of the solute was assumed to not require the displacement of solvent in the opposite direction. With this assumption, the force experienced by a solute should be independent of the susceptibility of the mobile phase. Secondly, the magnetic susceptibility of molecules are typically reported as a molar susceptibility, which combines the volume susceptibility and volume of a molecule. Hence, the modified equation for the purpose of solute migration in chromatography is shown in Equation 5.

$$F_{mag} = \frac{X_s . B . (\nabla B)}{\mu_0} \quad \text{(Equation 5)}$$

Where $\mathbf{X_s}$ is the molar susceptibility of the solute. The force experienced by the diamagnetic solute is therefore proportional to the magnetic flux and magnetic flux gradient.

3.3.2 Magnetic Simulations

The proof of concept experiment demonstrated that the nature of the magnetic environment directly affected whether solute migration from the walls was observed. The alternating orientation produced no solute migration, whereas the moving neodymium magnet and repeating magnet orientation provided a positive result. This is likely a result of more favourable magnetic flux densities and gradients at the column wall for these environments. In order to further understand the nature of these and other magnetic environments, 2-dimensional magnetic simulations were performed. It is important to stress the 2-dimensionality of these simulations and that the magnetic environments experienced by the column are 3-dimensional in nature. Hence the information from these simulations can only be used as a guide for designing and understanding the magnetic fields produced.

Single magnet arrays were selected for initial investigation to observe simple migration of the solute from one side of the column to the other. If successful, arrays could then be positioned both sides of the column to determine whether the solute is focused by diamagnetic repulsion toward the centre of the column. Three single array magnetic fields were simulated and are presented in Figure 14. Configuration (a) and (b) are the alternating and repeating orientations respectively. A third conformation (c) is also presented which was not trialled in the proof of concept experiments and utilises a 90 degree rotation between adjacent magnets.

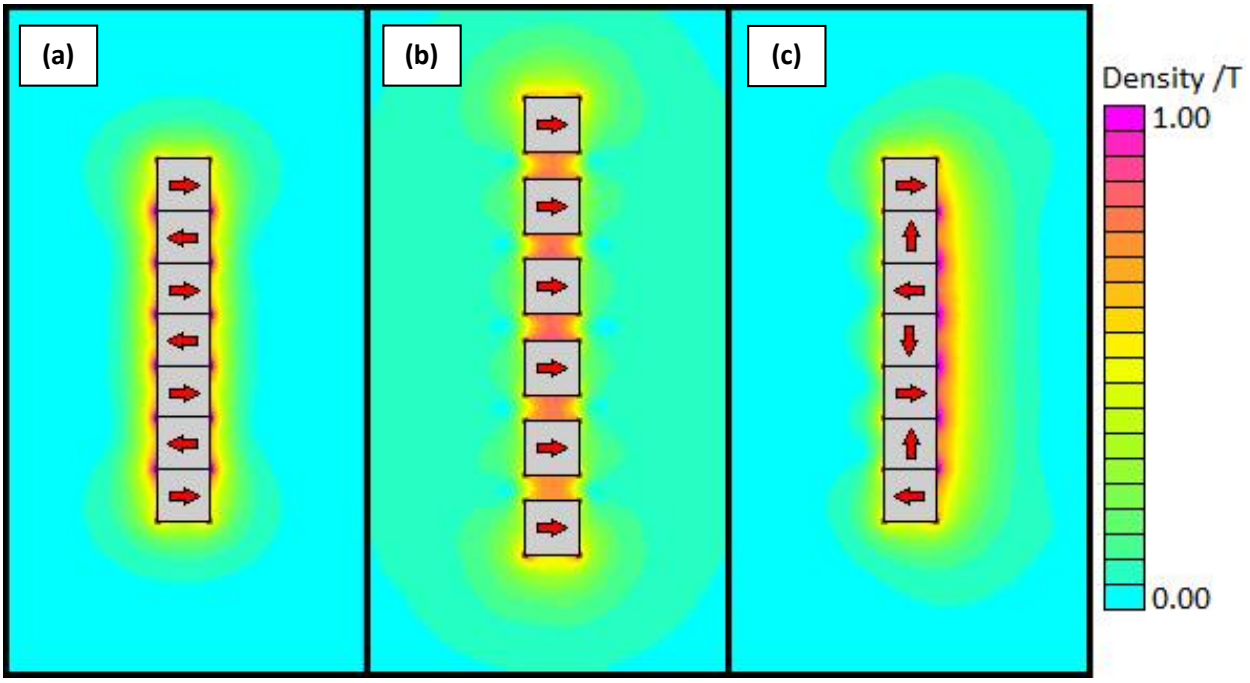

Figure 14: FEMM magnetic simulations of 10 mm x 10 mm N52 grade neodymium magnets (grey) with air as the surrounding medium. Red arrows indicate the direction of the magnets poles. Orientations simulated are (a) alternating, (b) repeating and (c) rotating.

The simulations are able to provide quantitative information regarding the intensities and gradients of magnetic flux caused by the magnetic orientations. The software had a limited selection of neodymium magnets grades available for simulation that did not match the grades used in subsequent experiments. Specifically N52 grade magnets were used for simulation, whereas N45 grade magnets were used experimentally. Hence, larger magnetic flux densities were calculated for the higher grade N52 magnets compared values measured experimentally for N45 grades.

The magnetic flux densities simulated for each orientation as a function of distance perpendicular to the magnet face, are presented in Figure 15. The flux profiles vary according to location on the magnet surface measured. Hence, simulation values were taken perpendicular to both the magnets centre and edge from each assembly.

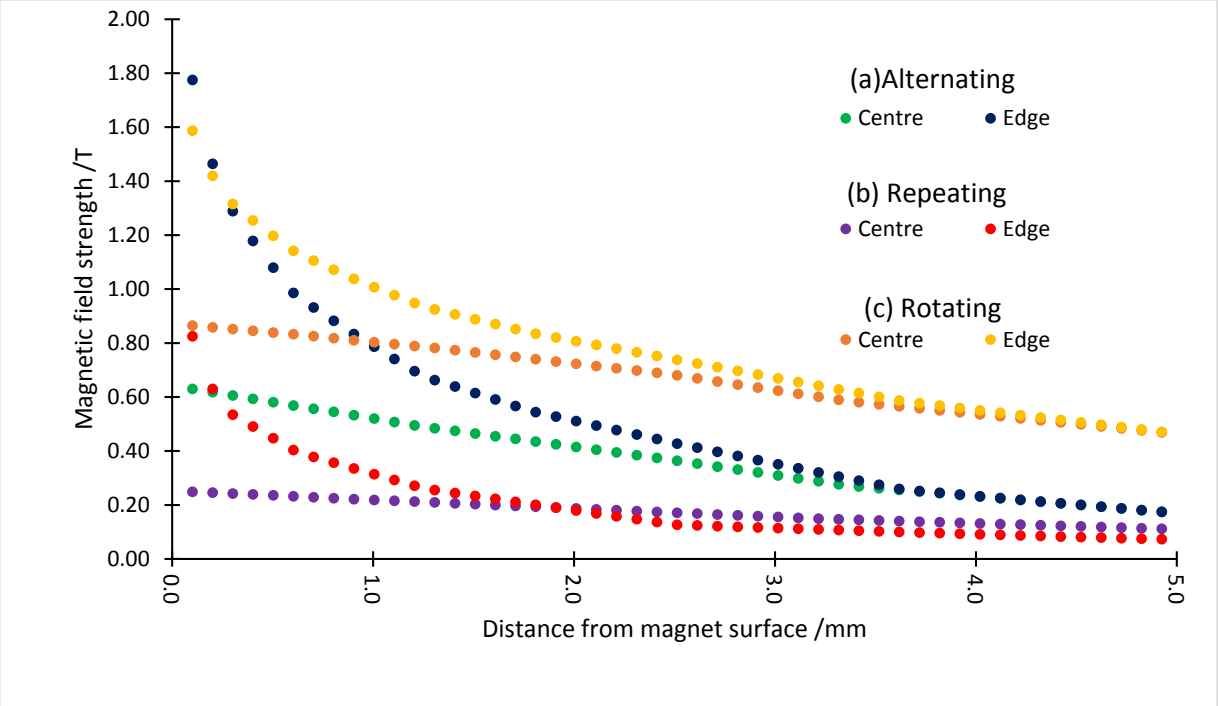

Figure 15: FEMM simulation data plotting the magnetic field strength as a function of distance from the magnet surface perpendicular to both the centre and edge of magnets in (a) alternating conformation, (b) repeating conformation and (c) rotating conformation.

The alternating orientation produces a magnetic flux which is concentrated at the edge of adjacent magnets. This would be experienced as pulses of magnetic field for a molecule travelling in the axial direction alongside the magnet assembly. A similar morphology in this sense is observed for the repeating orientation, with pulses of higher flux occurring at the magnet centres. However these pulses are relatively lower in magnetic flux, with the highest flux density occurring between the magnets as opposed to perpendicular from the array. The apparent lower flux density for the repeating orientation was unexpected considering its success in the proof of principle experiments. This may be the result of simulating a three dimensional problem in two dimensions. In two dimensions, the magnetic field lines are confined to a single plane, and are forced between the 5 mm gap of each magnet in the repeating orientation. However in reality, these field lines would be free to go around the magnet ‘out of the plane’ as opposed to be forced between adjacent magnets of the array.

With the limitations of the alternating and repeating conformations realised, the third conformation (c) was developed, utilizing a 90 degree rotation between adjacent magnets. Conformation (c) results in an additive effect taking place on one side of the array, and a subtractive effect taking place on the other side. This effect is observed in the simulation presented in Figure 14 (c). The morphology of the field is drastically different to the previous orientations, producing a more evenly distributed magnetic field as opposed to pulses in the axial direction. This orientation also produces stronger magnetic fluxes as a result of its additive effect. The higher magnetic flux density is also maintained at greater distances from the magnet surface, which may be advantageous for column formats with thicker walls.

3.3.3 Force Experienced by a Diamagnetic Solute

Using the magnetic gradients calculated from simulation data in combination with experimentally determined magnetic flux values, the force experienced by a diamagnetic solute can be calculated using Equation 5. These values are presented in Table 1 showing the force experienced by the iodine solute, with a molar susceptibility of -90×10^{-6} cm^3 mol^{-1}, at a distance of 3.5 mm. This length represents the distance of the stationary phase from the magnet surface and is the sum of the column wall thickness and magnet apparatus.

Table 1: Measured magnetic flux, simulated flux gradient and calculated diamagnetic force experienced by an iodine solute for three magnet orientations determined at 3.5 mm from the magnet's centre.

Orientation	**Maximum Measured Magnetic Flux* /T**	**Simulated Magnetic Flux Gradient /T m^{-1}**	**Calculated Diamagnetic Force /N mol^{-1}**
Alternating	0.2315 ±0.0023	62	1.0×10^{-3}
Repeating	0.2400 ±0.0024	22	3.8×10^{-4}
Rotating	0.4047 ±0.0040	74	2.1×10^{-3}

*uncertainties were calculated from the accuracy of the instrument (±1%).

The maximum measured magnetic flux was determined to be of similar magnitude for both the alternating and repeating orientations at a distance of 3.5 mm. This was surprising considering that no solute migration was observed for the alternating array. The simulated flux gradient is also higher for the alternating orientation. However, as discussed before, limitations of

the two dimensional simulations may have resulted in the underestimation of this value. The rotating orientation measured the largest magnetic flux and flux gradient out of all the orientations as predicted by the FEMM simulation. Consequently, the greatest diamagnetic force is calculated for this orientation compared to the other magnet arrays.

An example calculation for diamagnetic force experienced by an iodine molecule

The calculation below is for an iodine solute at a distance of 3.5 mm from an alternating magnet array.

$$F_{mag} = \frac{X_s . B . (\nabla B)}{\mu_0}$$

Values for each parameter are presented below showing conversion to SI units.

X_s	$= -90\times10^{-6}$ cm^3 mol^{-1}	B	= 0.2315 T
	$= -90\times10^{-12}$ m^3 mol^{-1}		=0.2315 kg C^{-1} s^{-1}
(∇B)	= 62 T m^{-1}	μ_0	$= 4\pi\times10^{-7}$ H m^{-1}
	= 62 kg C^{-1} s^{-1} m^{-1}		$= 4\pi\times10^{-7}$ kg m C^{-2}

$$F_{mag} = \frac{(-90\times10^{-12}\ m^3\ mol^{-1})(0.2315\ kg\ C^{-1}\ s^{-1})(62\ kg\ C^{-1}\ s^{-1}\ m^{-1})}{(4\pi\times10^{-7}\ kg\ m\ C^{-2})}$$

$$F_{mag} = \frac{(-90\times10^{-12}\ m^{\cancel{3}}\ mol^{-1})(0.2315\ \cancel{kg}\ \cancel{C^{-1}}\ s^{-1})(62\ kg\ \cancel{C^{-1}}\ s^{-1}\ \cancel{m^{-1}})}{(4\pi\times10^{-7}\ \cancel{kg}\ \cancel{m}\ \cancel{C^{-2}})}$$

$$F_{mag} = \frac{(-90\times10^{-12}\ )(0.2315)(62)}{(4\pi\times10^{-7})}\ kg\ m\ s^{-2}\ mol^{-1}$$

$$F_{mag} = \frac{(-90\times10^{-12}\ )(0.2315)(62)}{(4\pi\times10^{-7})}\ N\ mol^{-1}$$

$$F_{mag} = -1.0\times10^{-3}\ N\ mol^{-1}$$

The sign indicates the direction of the force. Negative indicates force away from the region of high magnet flux. Forces are presented as their absolute values in text.

In the presence of these magnet arrays, the diamagnetic solute experiences a net directional force away from the wall of the column. As the iodine is repelled from the walls of the chromatography column according to this force, the molecule experiences a viscous drag force in the opposite direction. The magnitude of this force is calculated using Equation 6.

$$F_{vis} = \frac{1}{2}.\rho.v^2.C_D.A \text{ (Equation 6)}$$

Where $\mathbf{F_{vis}}$ is the drag force, $\boldsymbol{\rho}$ is the density of the mobile phase, $\mathbf{v}$ is the velocity of the molecule, $\mathbf{C_D}$ is the drag coefficient and $\mathbf{A}$ is the cross sectional area. By considering the magnetic forces and drag forces experienced by the solute, the total acceleration of the iodine molecule from the column wall can be calculated using Equation 7.

$$a = \frac{\frac{F_{mag}}{N_A} - F_{vis}}{m} \text{ (Equation 7)}$$

Where $\mathbf{a}$ is the acceleration of the iodine molecule, $\mathbf{m}$ is the mass of the iodine molecule and $\mathbf{N_A}$ is Avogadro's number (6.022×10^{23} mol^{-1}). As the solute accelerates away from the column wall, the drag forces in the opposite direction to the migration increases proportionally to the square of the velocity (Equation 6). At a critical velocity, $\mathbf{F_{vis}}$ will reach an equivalence with $\mathbf{F_{mag}}$ and acceleration of the iodine will become zero. This is expressed in Equation 8 below.

$$\frac{X_s.B.(\nabla B)}{\mu_0.N_A} = \frac{1}{2}.\rho.v^2.C_D.A \text{ (Equation 8)}$$

Through simple rearrangement, the critical velocity for the solute can then be calculated by using Equation 9 below.

$$v = \sqrt{\frac{2.X_s.B.(\nabla B)}{\mu_0.N_A.\rho.C_D.A}} \text{ (Equation 9)}$$

The critical velocity of the solute is therefore proportional to the square root of magnetic flux and magnetic flux gradient. Using this information the migration of the iodine solute from the column wall can then be plotted as a function of time. Calculation using this method requires a number of assumptions to be made. These assumptions and their justifications will be discussed in following example calculation.

The calculated migration of the iodine solute for each conformation with a magnet distance of 3.5 mm is presented in Figure 16. The rotating conformation, due to its larger magnetic flux and gradient previously discussed, is calculated to provide the greatest migration from the column wall. Within two minutes, solute molecules near the wall are expected to migrate over 1 mm towards the column centre. In the case of a standard 4.6 mm ID HPLC column, assuming the same magnetic flux and gradients are achieved, this distance represents over 40% of the column radius. As the wall effects typically affect the outer 20% of the column (see Figure 1), the calculation reaffirmed the positive result from the proof of principle as a potential method to mediate the wall effects.

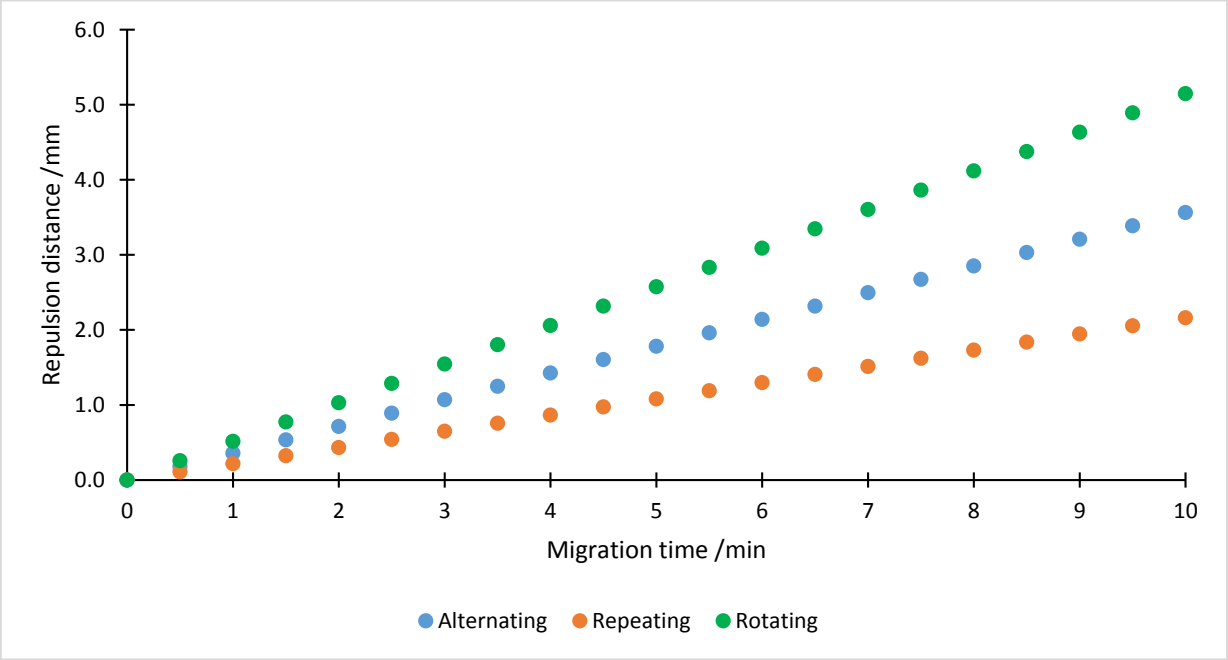

Figure 16: Plot showing the migration distance of an iodine molecule as a function of time calculated using Equation 9. Migration is plotted for an alternating (blue), repeating (orange) and rotating (green) magnet orientation.

An example calculation for the expected migration of an iodine molecule

The calculation below is for an iodine molecule at a distance of 3.5 mm from an alternating magnet array.

There are three assumptions used in the calculation of an iodine molecule's migration.

The first assumption is that maximum velocity of the solute is achieved at time zero. This assumption has been justified by calculating the acceleration of the iodine solute shown below.

$$a = \frac{F_{mag}}{m.N_A}$$

Where $\boldsymbol{a}$ *is the acceleration of the molecule and* $\boldsymbol{m}$ *is the mass of an iodine molecule.*

F_{mag}	$= 1.7\times10^{-27}$ N	m	$= 4.21\times10^{-25}$ kg
N_A	$= 6.022\times10^{23}$ mol^{-1}		

$$a = \frac{-1.0 \times 10^{-3}\ \text{N mol}^{-1}}{(4.21 \times 10^{-25}\ \text{kg})(6.022 \times 10^{23}\ \text{mol}^{-1})}$$

$$a = \frac{-1.0 \times 10^{-3}\ \text{kg m s}^{-2}\ \text{mol}^{-1}}{(4.21 \times 10^{-25}\ \text{kg})(6.022 \times 10^{23}\ \text{mol}^{-1})}$$

$$a = \frac{-1.0 \times 10^{-3}\ \cancel{\text{kg}}\ \text{m s}^{-2}\ \cancel{\text{mol}^{-1}}}{(4.21 \times 10^{-25}\ \cancel{\text{kg}})(6.022 \times 10^{23}\ \cancel{\text{mol}^{-1}})}$$

$$a = \frac{-1.0 \times 10^{-3}}{(4.21 \times 10^{-25})(6.022 \times 10^{23})}\ \text{m s}^{-2}$$

$$a = 0.0041\ \text{m s}^{-2}$$

The acceleration is approximately 3 orders of magnitude greater than the critical velocity. Hence the time taken to reach maximum velocity was considered negligible and not included in the calculation.

The second assumption is that magnetic flux and gradient do not change significantly over the distance of solute migration. This assumption was primarily made to maintain the simplicity of the calculation and may lead to slight over-estimation of the migration.

The final assumption regards the treatment of the iodine molecule. Iodine molecules are treated as spheres with radii equal to the van der Waals radii of the molecule (203 pm) [51]. This also has implications for the drag coefficient (C_D) used which is 0.47 for spherical objects.

Calculation of the critical velocity was as follows:

$$v = \sqrt{\frac{2.X_s.B.(\nabla B)}{\mu_0.N_A.\rho.C_D.A}}$$

X_s	$= -90\times10^{-12}$ m^3 mol^{-1}	B	$= 0.2315$ kg C^{-1} s^{-1}
(∇B)	$= 62$ kg C^{-1} s^{-1} m^{-1}	μ_0	$= 4\pi\times10^{-7}$ kg m C^{-2}
N_A	$= 6.022\times10^{23}$ mol^{-1}	ρ	$= 1590$ kg m^{-3}
C_D	$= 0.47$	A	$= \pi\times(203\text{ pm})^2$
			$= 1.3\times10^{-19}$ m^2

$$v = \sqrt{\frac{2(-90 \times 10^{-12}\ m^3\ mol^{-1})(0.2315\ kg\ C^{-1}\ s^{-1})(62\ kg\ C^{-1}\ s^{-1}\ m^{-1})}{(4\pi \times 10^{-7}\ kg\ m\ C^{-2})(6.022 \times 10^{23}\ mol^{-1})(1590\ kg\ m^{-3})(0.47)(1.3 \times 10^{-19}\ m^2)}}$$

$$v = \sqrt{\frac{2(-90 \times 10^{-12}\ \cancel{m^3}\ \cancel{mol^{-1}})(0.2315\ \cancel{kg}\ \cancel{C^{-1}}\ s^{-1})(62\ \cancel{kg}\ \cancel{C^{-1}}\ s^{-1}\ \cancel{m^{-1}})}{(4\pi \times 10^{-7}\ \cancel{kg}\ \cancel{m}\ \cancel{C^{-2}})(6.022 \times 10^{23}\ \cancel{mol^{-1}})(1590\ \cancel{kg}\ m^{-2})(0.47)(1.3 \times 10^{-19}\ \cancel{m^2})}}$$

$$v = \sqrt{\frac{2(-90 \times 10^{-12})(0.2315)(62)}{(4\pi \times 10^{-7})(6.022 \times 10^{23})(1590)(0.47)(1.3 \times 10^{-19})}\ m^2\ s^{-2}}$$

$$v = \sqrt{3.5 \times 10^{-11}\ m^2\ s^{-2}}$$

$$v = 6.0\ \times 10^{-6}\ m\ s^{-1}$$

at t = 300 seconds

$$d = v \times t$$

$$d = 6.0\ \times 10^{-6}\ m\ s^{-1} \times 300\ s$$

$$d = 0.0018\ m = 1.8\ mm$$

3.4 On-column visualisation using a 15 mm ID column

3.4.1 Solute migration analysis using on-column visualisation

Figure 17: Solute profile of a 50 µL injection of 12 g L^{-1} iodine CTC solution on a 15 mm ID column 7 minutes into its elution.

For the analysis of solute migration in the presence and absence of magnetic fields, a 15 mm ID borosilicate column was initially trialled. Packing the column in a reproducible manner proved difficult, with solute band morphology observed to be inconsistent between packed columns. However, it was the change in morphology that was of interest as opposed to the shape itself. Hence, the selection criteria of a column was whether the band morphology was reproducible between injections. The morphology of the solute profile in the absence of magnets in shown in Figure 17. The profile is slightly slanted towards the right and a tail-like distortion near the profiles centre. Replicate injections on the column demonstrated that the band morphology was highly reproducible and was deemed suitable for the analysis.

Analysis of the solute band using image analysis software allows various profile characteristics to be determined at any point of the iodine's elution. Images were initially converted to 8-bit grayscale before having a background image subtracted. The result

is the solute profile as a series of numbers corresponding to each pixel of the image. These numbers, called the grayscale intensity, are within the range of 0 and 255 and are a function of the iodine concentration within the column. Low values indicate the absence or low concentration of iodine, whereas higher values indicate high iodine concentration.

For quantitative analysis of the iodine solute, calibrations curves would have to be constructed for the column. This would be performed by pumping iodine solutions of various concentrations through the column and plotting the grayscale intensity as a function of concentration. As the path length of the sample cell (in this case the column) changes with radial location, calibration curves would need to be constructed for the different radial locations of the column. In this study, the changes in grayscale intensity were initially measured before calibration performed to determine if any net effect had occurred. Calibration curves would only be required after diamagnetic repulsion is achieved to quantify the effect. This would have to be performed for the specific conditions of the analysis.

The simplest feature of the solute band that can be calculated is its peak profile as would be measured by a post-column detector. This was performed by averaging the transverse grayscale intensities of the profile and plotting these values as a function of axial distance. The peak profiles of duplicate runs using a 50 µL injection 7 minutes into its elution are shown in Figure 18. A good degree of reproducibility was achieved between replicates with near identical peak profiles. Only small differences were observed in the tailing portion of the profile.

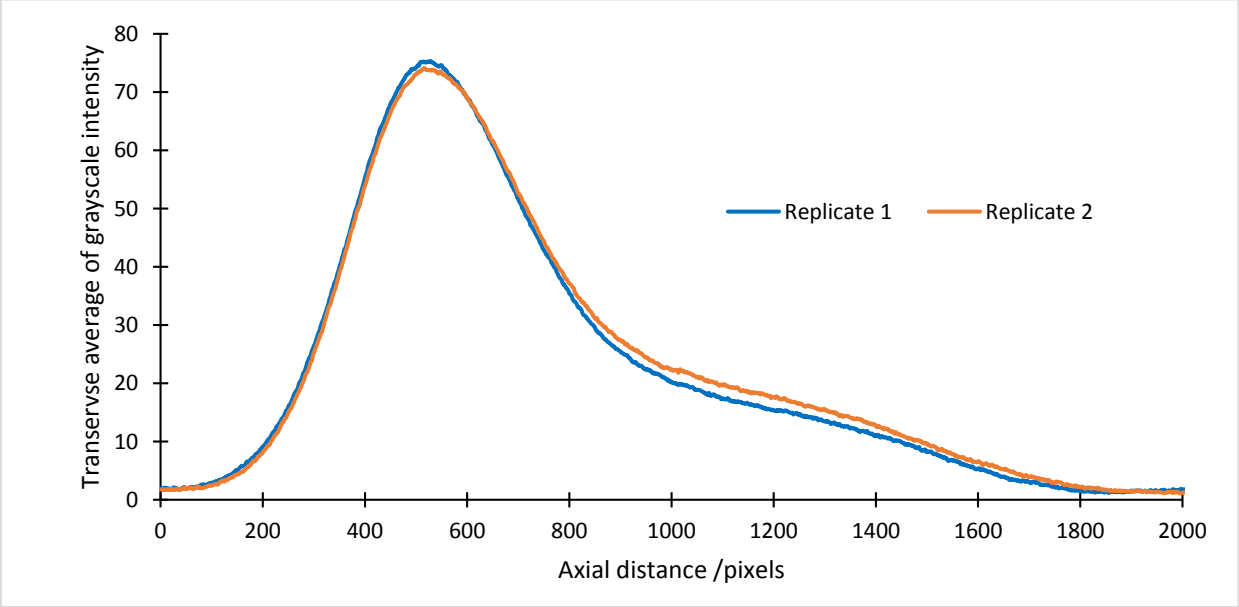

Figure 18: Peak profiles of duplicate injections of 50 µL 12 g L^{-1} iodine in CTC on a 15 mm ID column after 7 minutes. Peak is plotted using the average of the transverse grayscale intensity versus axial pixel distance.

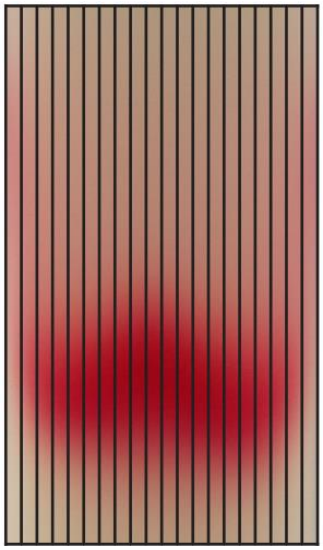

Figure 19: Diagram showing the division of the iodine solute profile into 20 individual vertical bands.

For a more informative analysis, the solute profile can be subdivided into bands that sample the axial direction of the column, allowing peaks to be calculated for different radial locations of the column. As illustrated in Figure 19, the solute profile was divided into 20 individual vertical bands with a width of 46 ±1 pixels. Herein, each band will be referred as a normalized value between -1 and 1 with 0 representing the radial centre of the column and ±1 representing the radial extremities of the column either side. Similar to the bulk peak profile, transverse values within each band were averaged and plotted as a function of axial distance shown in Figure 20.

Plotting the transverse grayscale intensity average as a function of pixel distance initially produced radial chromatograms with a low signal to noise ratio of 21 for the outermost radial band. To reduce the noise of the chromatograms, the grayscale intensity was plotted as the adjacent average of 20 successive points. This increased the signal to noise ratio to 81. Figure 20 and all subsequent radial chromatograms are plotted using the 20 adjacent average grayscale.

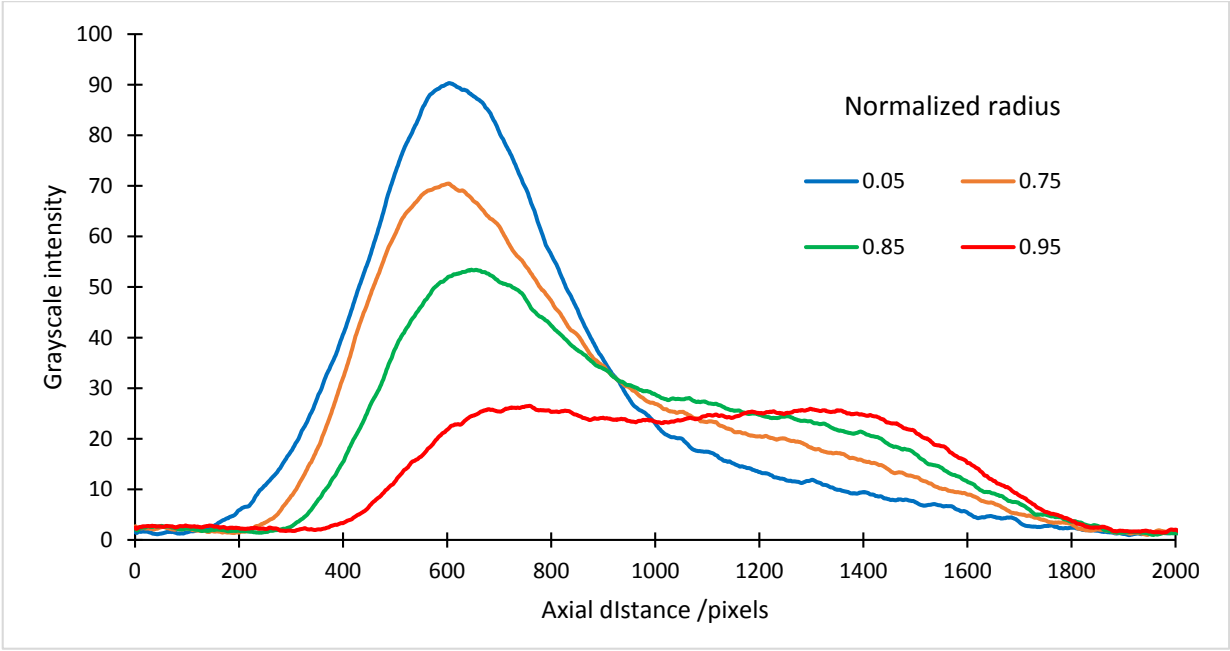

Figure 20: Radial chromatograms of a 50 µL injection of 12 g L^{-1} iodine in CTC on a 15 mm ID column after 7 minutes. Radial chromatograms shown are at normalized radial locations 0.05 (blue), 0.75 (orange), 0.85 (green) and 0.95 (red).

The radial chromatograms for the 50 µL injection highlight importance differences in peak shape as a function of radial distance. Peaks measured for the central portion of the column were narrower with less tailing compared to those measured near the column wall. The narrower radial peak shape remained similar between radial locations of -0.65 and 0.65. At the outer portion of the column, peaks began to broaden and the tailing aspect of the peak became more predominant. This begins to occur over reduced radii of ±0.75 to ±0.95 where, as shown in Figure 20, peak shape becomes severely distorted as the wall is approached. This illustrates the peak broadening and tailing contributions made by the frictional wall effect at the peripheral portion of the column. An abnormal peak profile was observed at the outermost radial band of the profile, showing a splitting feature causing two apexes. This morphology was consistent at both the left and right sides of the solute band and between replicates.

The radial chromatograms can be further processed using Simpson's integration to calculate the distribution of the solute across the diameter of the column. The solute distribution for replicate analysis of a 50 µL injection in the absence of magnets, normalized to the largest peak area, is presented in Figure 21. The sample is preferentially loaded in the central portion of the packing with lower grayscale intensity measured at the column walls. The distribution of the iodine is also slightly asymmetrical across the diameter of the column, with a higher concentration measured at the right hand side of the column compared to the left. Nonetheless, good agreement between the duplicate injections was achieved particularly for the central portion of the column. Small differences in normalized peak area were measured at outer radii values.

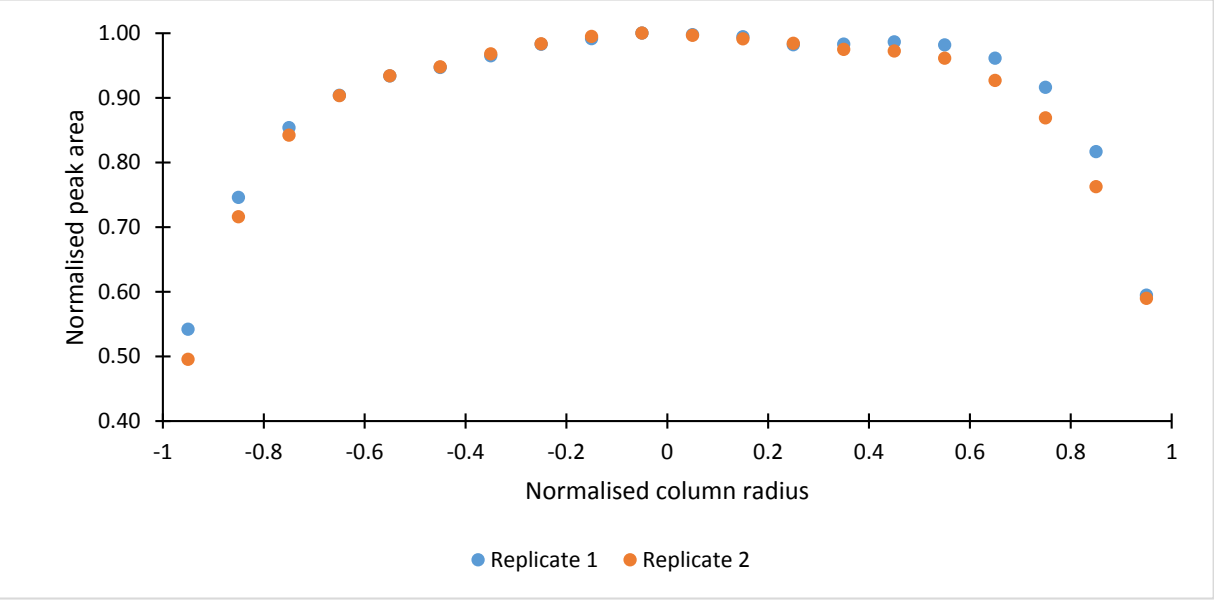

Figure 21: Normalized solute distribution of iodine for duplicate injections of 50 µL 12 g L^{-1} iodine in CTC across the diameter of a 15 mm ID column after 7 minutes.

3.4.2 Solute migration in the presence of a rotating magnet orientation

With concerns over the distance of the magnets from the column packing, the rotating orientation was initially trailed as it was predicted to produce the largest diamagnetic force for an iodine molecule at a distance of 3.5 mm. An 8 magnet array was assembled which extended from approximately 5 mm above the inlet frit to the outlet frit of the column. Only the left side of the magnet apparatus was loaded with magnets. If diamagnetic repulsion was achieved by the application of magnets, a shift in solute distribution across the diameter of the column should be measured. That is, Simpson's integration of peaks at radial locations near the magnets will produce lower values, whereas radial locations further from the magnets will measure higher grayscale values. A change in peak shape of the axial bands closest the magnet array would also be expected if repulsion was successful.

Comparison of the solute profiles was performed 7 minutes after the injection of the iodine solution. This time was selected as it was the maximum time the iodine remained on the column before reaching the outlet frit. This would allow the solute maximum exposure to the magnet array and give the strongest indication if diamagnetic repulsion was achieved. If achieved, the change in peak shape and solute distribution could be analysed over the solutes entire elution.

Previous calculations, presented in Figure 16, predicted a distance of 3.6 mm to be generated between the column wall and the iodine solute at 7 minutes into its elution. This would be interpreted as no significant grayscale intensity being measured between the normalized radii of -0.65 and -0.95, with reduced grayscale intensity at -0.55. Importantly, this is the portion of the column, determined by the radial chromatograms in Figure 20, to be most affected by the frictional wall effect and contributed considerably to the tailing portion of the bulk peak.

Following injection in the absence and presence of the rotating magnetic field, there appeared no visual change for the iodine solute profile. Peak profiles of the two axial bands closest the magnet array (-0.95 and -0.85) are shown in Figure 22 for both the no magnet and rotating duplicates.

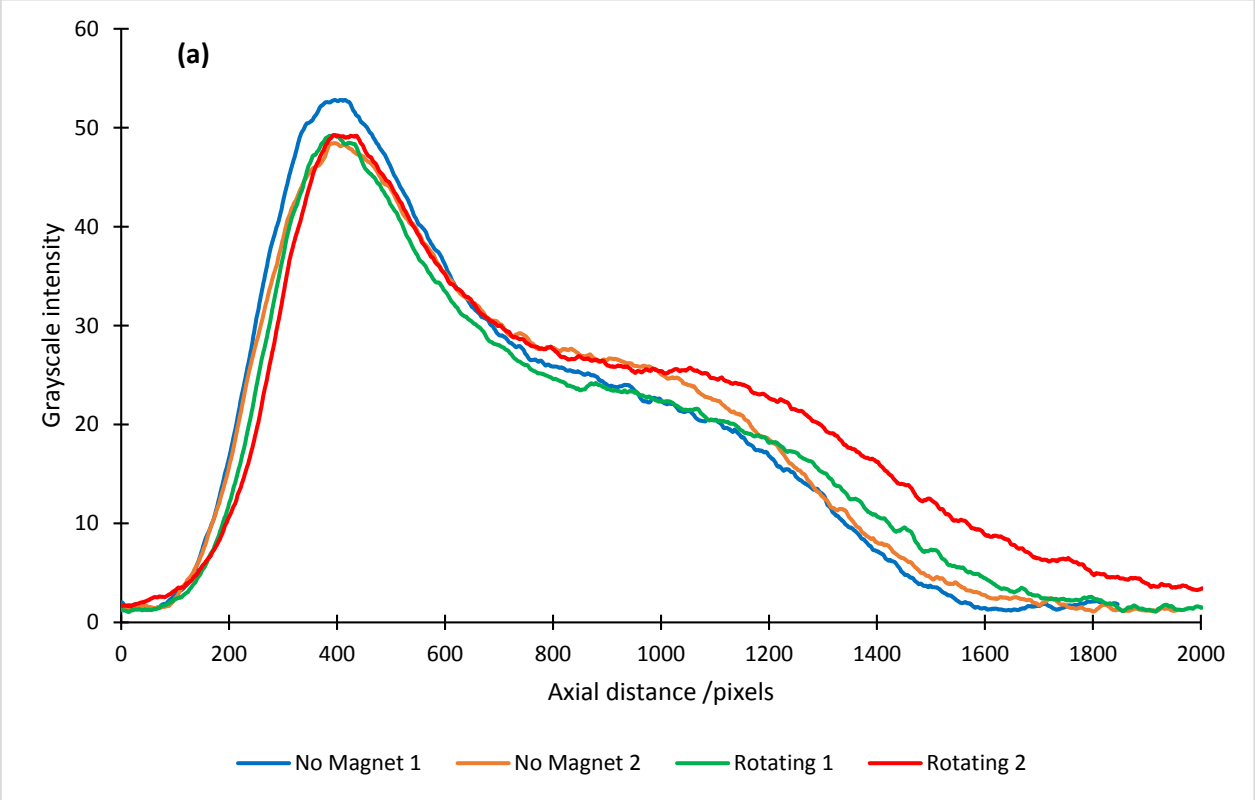

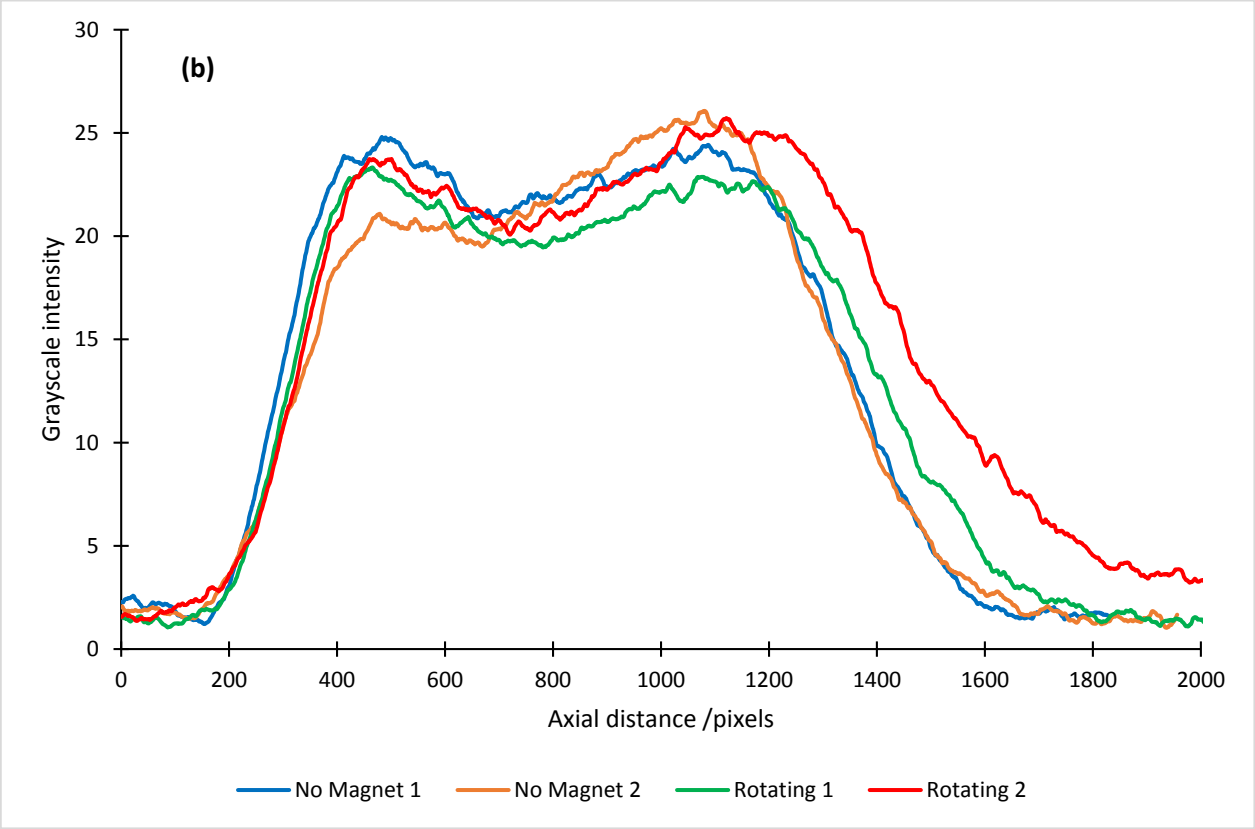

Figure 22: Radial chromatograms of 50 µL injections of 12 g L^{-1} iodine in CTC on a 15 mm ID column at normalized radii of (a) -0.85 and (b) -0.95 after 7 minutes. Radial chromatograms are presented for elution in the absence of magnetic fields (blue and orange) and in the presence of a rotating magnet orientation (green and red).

Analysis of the chromatograms at normalized radii of -0.95 and -0.85 showed little change in peak shape for either band. An increase in tailing was observed for profiles measured in the presence of magnets, however this appears to be the result of a drift in column performance, as tailing increased in order of analysis sequence. For the outermost radial band of -0.95, the splitting feature of the peak was observed in both blank and magnet runs with no significant difference in peak height measured. This indicated that diamagnetic repulsion of the iodine solute was not achieved through the application of the rotating magnet conformation. The negative result was confirmed through Simpson's integration of the peaks across the diameter of the column shown in Figure 23.

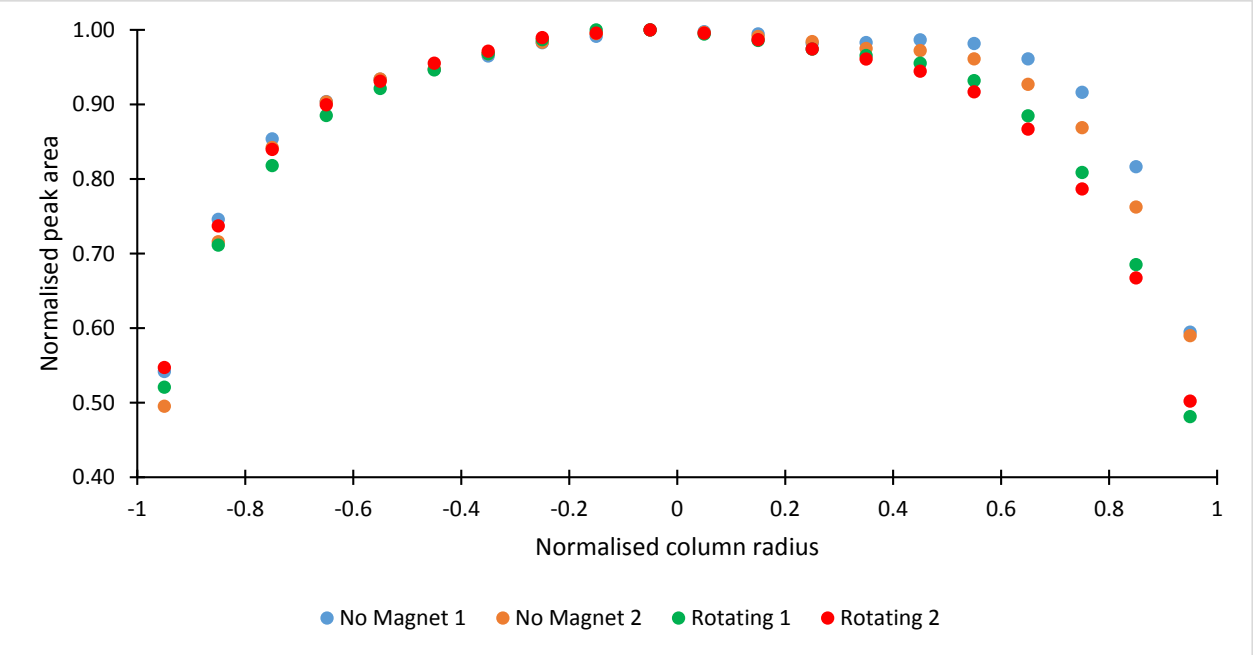

Figure 23: Normalized solute distribution of iodine across the dimeter of a 15 mm ID column as determined by Simpson's Integration in the absence of magnetic fields (blue and orange) and in the presence of a rotating magnet orientation (green and red) after 7 minutes. Magnetic field was positioned to the left (negative) side of the column.

Normalized distributions of the iodine solute showed no significant change at locations near the magnet array. Changes were observed for the right-hand side of the column, where relatively higher concentrations of iodine were measured for runs in the absence of magnets. This region of the column is furthest from the magnets and hence is not likely a product of the magnetic environment. Rather, this difference may indicate a drift in the column performance.

As no migration was observed on the 15 mm ID chromatography column, assessment of the previous calculations was required. A large overestimation of the iodine's migration in the column was calculated for the rotating conformation at a distance of 3.5 mm. Where Equation 9

predicted a migration distance of 3.6 mm, none was observed. This may have been a result of the assumptions made in the calculation or the exclusion of other factors that may affect the migration. For example, the stationary phase itself may inhibit migration of the solute away from the column walls. For this reason, subsequent calculations only addressed the diamagnetic force directly experienced by the solute and were not further processed to predict migration distances.

The differences between the results of proof of principle experiments and the on-column visualisation experiments were also assessed to discern whether they were the cause of the discrepancy. The thickness of the column walls was of major concern, as magnetic flux and flux gradient decay rapidly with increasing distance from the magnet surface. An increase in distance from 0.5 mm in the proof of concept experiments to 3.5 mm was identified as a probable cause of the negative result for the 15 mm ID column.

Despite no diamagnetic repulsion being observed, the chromatography system proved effective in visualising solute migration using the principle of matched refractive indices. Peak shape was found to be highly reproducible between replicate analyses. Further subdivision of the profile into radial chromatograms also showed good reproducibility regarding peak shape and peak area. The greatest source of error between replicate analyses appeared to be shifts in the column performance, which increased peak tailing and caused small changes in solute distribution between replicate analyses.

3.5 On-column visualisation using a 4.0 mm ID column

3.5.1 Revisions of Chromatography System

With no solute migration measured using the 15 mm ID column format, revisions were made to the chromatography system with the objective to minimize the distance between the magnet array surface and the column packing. As no borosilicate chromatography columns were available with wall thicknesses below 2.5 mm, a custom glass column format was required. The new column was designed to mimic that of a standard HPLC column. A borosilicate tube with an ID of 4.0 mm and wall thickness of 1.0 mm was cut to a length of 100 mm. The ends of the column were capped with ¼ inch Swagelok fittings that each housed a 2 µm steel frit. Tubing could then be connected to the column as per standard HPLC. The magnet apparatus was also modified to remove the central portion of the 1 mm polyacetal plastic layer that secured the magnets allowing their direct contact with the column wall. Overall the modifications resulted in a reduction in

Figure 24: Image showing the constructed 4.0 mm column and modified magnet apparatus.

magnet distance from 3.5 mm to 1.0 mm, bringing the magnets much closer to the 0.5 mm of the proof of concept column. The 4.0 mm ID column with the modified magnetic apparatus is shown in Figure 24.

Recalculation of the force experienced by the solute at a distance of 1.0 mm is presented in Table 2. The measured magnetic flux for all conformations was measured as approximately 0.2 T higher compared to 3.5 mm. Conversely, the magnetic flux gradient remained relatively constant for the conformations except for the alternating conformation which significantly increased. This increased the calculated diamagnetic force experienced by the solute by 280%, 120% and 45% for the alternating, repeating and rotating conformations respectively. At a distance of 1.0 mm, the alternating orientation provided the greatest theoretical diamagnetic force, followed by the rotating and repeating conformations.

Table 2: Measured magnetic flux, simulated flux gradient and calculated diamagnetic force experienced by an iodine solute for three magnet orientations determined at 1.0 mm from the magnet's centre. Calculated diamagnetic force at 3.5 mm for each conformation is also presented.

Orientation	**Maximum Measured Magnetic Flux* /T**	**Simulated Magnetic Flux Gradient /T m^{-1}**	**Calculated Diamagnetic Force at 1.0 mm /N mol^{-1}**	**Calculated Diamagnetic Force at 3.5 mm /N mol^{-1}**
Alternating	0.4337 ±0.0043	126	3.9×10^{-3}	1.0×10^{-3}
Repeating	0.4024 ±0.0040	30	8.6×10^{-4}	3.8×10^{-4}
Rotating	0.6194 ±0.0062	70	3.1×10^{-3}	2.1×10^{-3}

*uncertainties were calculated from the accuracy of the instrument (±1%).

3.5.2 Solute migration in the presence of magnetic fields

Packing of the 4.0 mm ID borosilicate proved difficult in comparison to the 15 mm ID column. Column performance was found to decay over time, with dead space often forming at the inlet frit. This was a direct result of the packing procedure. Higher flow rates were unable to be used to consolidate the bed due to the low pressure rating of the borosilicate column. At high flowrates, leaks would occur at the column inlet and outlet caps. Also as no adjustable column inlet was used, the stationary phase could not be axially compressed to prevent the formation of voids. This issue was only able to be partially addressed by leaving the columns to settle for 48 hours after initial consolidation, before a second consolidation performed. This ultimately produced broader solute profiles imaged by the chromatography system.

An increased optical zoom was required to achieve the desired resolution of the chromatography column. As a consequence, the axial distance of the column that could be sampled was also reduced. The number of radial bands for the column was also reduced from 20 to 10 with a width of 37 ±2 pixels. Due to the increased optical zoom and broad solute profiles, the solute profile was unable to be imaged in its entirety. An image of the profile shown in its inverse colours is presented in Figure 25. This was undesirable, as it required analysis to neglect the tailing portion of the profile. However it was deemed acceptable, as the most predominant change in solute profiles observed for the proof of principle experiments occurred at the peak front.

Figure 25: Solute profile of a 10 µL injection of 12 g L^{-1} iodine in CTC solution on a 4.0 mm ID column 2 minutes into its elution.

To evaluate diamagnetic repulsion on the 15 mm ID column in Section 3.4, peak shape at the column wall and distribution of the solute across the diameter of the column were both analysed. With concerns over the decay of column performance that accompanied packed 4.0 mm ID columns, a performance check was implemented to determine the change in these column features over the analysis period. Specifically, duplicate injections in the absence of magnetic fields were performed both before and after analysis to be compared. As would be expected with degrading performance, peak shape was observed to change significantly over the analysis time, with broader peaks measured post analysis. As a result, any change in peak shape between different magnetic environments could not be directly attributed to diamagnetic repulsion, and hence not evaluated for these injections. However, distribution of the solute across the column

diameter was found to be consistent both pre and post analysis. The distribution of duplicate runs performed before and after analysis is shown in Figure 26.

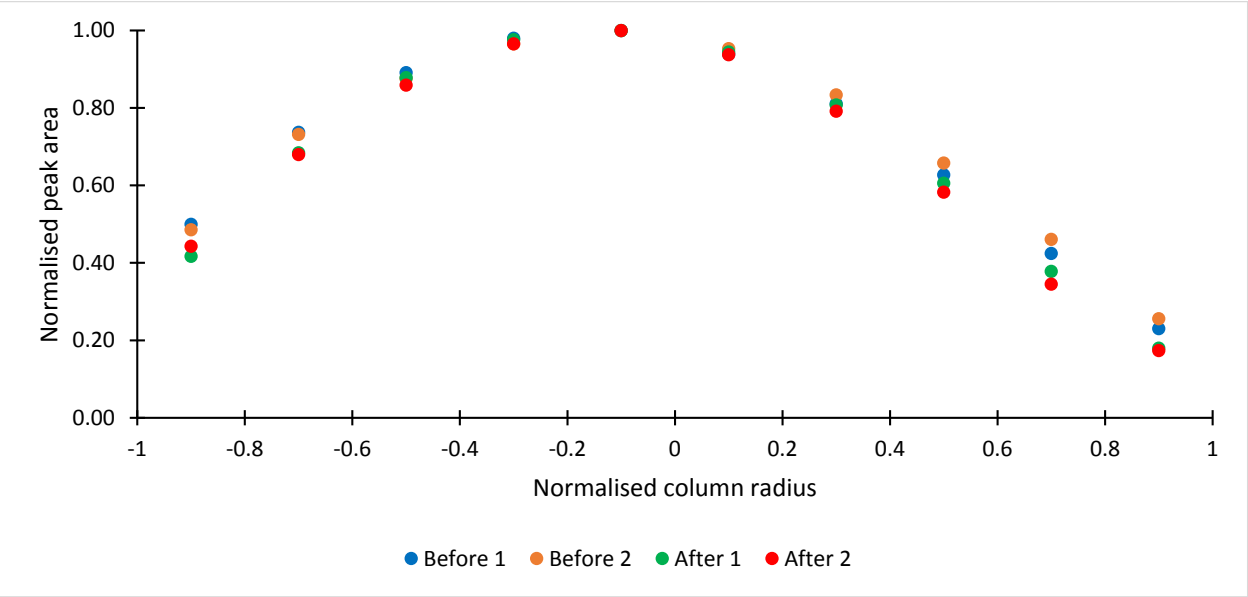

Figure 26: Performance check showing the normalized solute distribution of iodine across the diameter of a 4.0 mm ID column after 2 minutes. Distributions are shown for duplicate 10 µL injections of 12 g L^{-1} iodine in CTC performed before (blue and orange) and after (green and red) solute migration analysis runs.

The distribution of the iodine is asymmetric across the column diameter, with a higher loading of solute on the left hand side. This is consistent for duplicates performed both before and after solute migration analysis runs. However, small changes are observed near the wall region of the column for both sides. For the duplicate injections before analysis, the iodine is loaded slightly higher at the peripheral portions of the column compared to duplicate injections performed after analysis. This drift in solute distribution was expected to be small in comparison to the shift that would be observed if diamagnetic repulsion was achieved.

The left hand side of the column, which measured a higher solute loading, was selected for the positioning of neodymium magnets. Solute migration was analysed in the presence of the repeating, rotating and alternating conformations in the order listed, followed by the absence of magnets. The alternating and rotating orientations consisted of six 10 mm × 10 mm× 10 mm neodymium magnets with no space between adjacent magnets. The repeating, due to their repulsive orientation, consisted of 5 neodymium magnets separated by approximately 4-5 mm. The Swagelok fittings of the 4.0 mm column prevented magnets from being positioned at the inlet frit. Instead the magnet arrays were positioned immediately after the Swagelok cap. This meant that the solute travelled for approximately 10 mm in the stationary phase before becoming perpendicular with the magnet arrays.

The solute distributions of a 10 uL injection in the presence of each magnetic field and in the absence of magnetic fields are presented in Figure 27. The analysis measured no significant change in solute concentration at the left hand side of the column. The changes measured, which are within the experimental uncertainty, likely arose due to the order in which they were performed. The drift in performance discussed previously showed increased solute loading at the wall region for earlier analyses (repeating) compared to later analysis (no magnet).

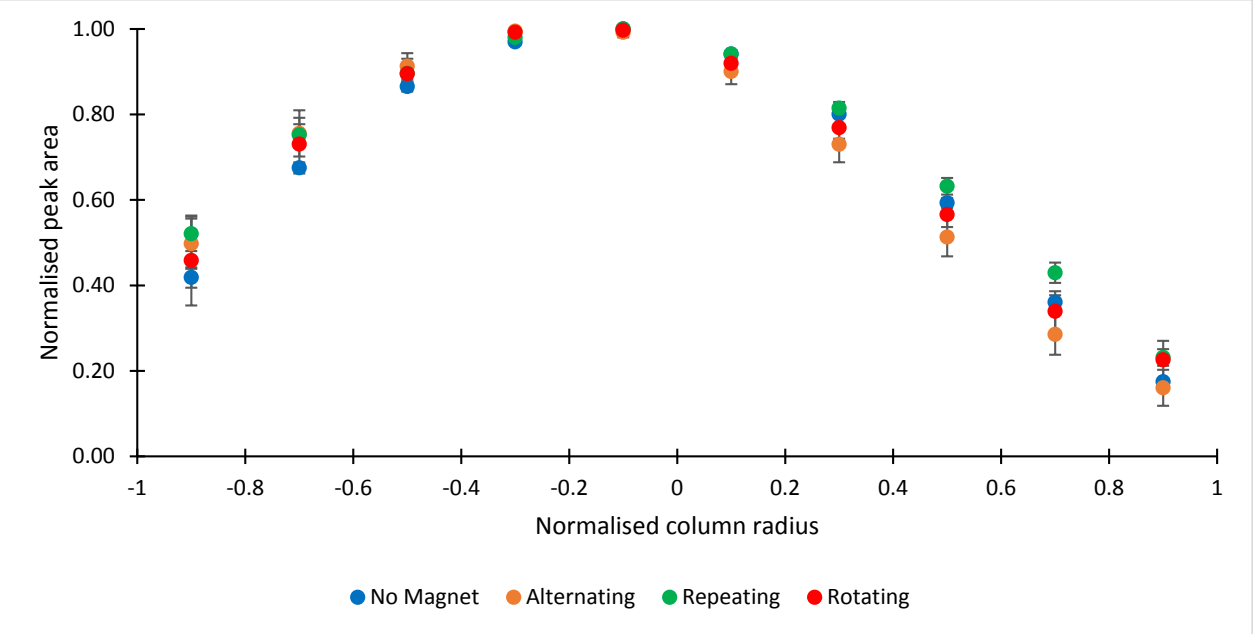

Figure 27: Normalized solute distribution of a 10 µL injection of 12 g L^{-1} iodine in CTC across the diameter of a 4.0 mm ID column after 2 minutes. Distribution was calculated for elution in the absence of magnetic fields (blue) and in the presence of a alternating (orange), repeating (green) and rotating (red) conformation. Data points represent the average of the triplicate analysis and error bars representing the standard deviation of the triplicate injections.

The solute distribution analysis indicates that the reduction in magnet distance using the 4.0 mm ID column was unable to produce a measurable diamagnetic repulsion using the on-column visualisation system. This indicates the thicker column walls of the 15 mm ID column may not have been the specific cause of the negative result obtained previously. Further modifications to the system were therefore required to minimize other differences that persisted between the proof of concept runs and the chromatography system.

The results, despite being negative, have demonstrated the on-column visualisation system was translatable to smaller column formats. Good agreement regarding solute distribution of the column was observed on the same packed column. However, limitations were experienced in its ability to analyse peak shape. This was not a function of the system itself but of the column which, due to its construction, is unable to be effectively packed.

3.5.3 Revisions of Chromatography System 2

Secondary revisions to the chromatography system were implemented to match the conditions initially trialled in the proof of concept experiments. The next most significant change between the experiments, following the column dimensions, was the mobile phase used. Mobile phases were changed between the experiments primarily for the requirements of on-column visualisation. A CTC mobile phase was used under the assumption that diamagnetic force is independent of the mobile phase, as discussed in section 3.3.1. If incorrect, the diamagnetic susceptibility of the mobile phase must be subtracted from that of the solute. This relationship was presented earlier in in Equation 4 and is re-presented below in Equation 10 to include the molar susceptibility of the mobile phase.

$$F_{mag} = \frac{(X_s - X_p).\,B.\,(\nabla B)}{\mu_0} \quad \text{(Equation 10)}$$

Where $\mathbf{X_p}$ is the molar susceptibility of the mobile phase.

CTC has a higher negative molar susceptibility of -66.8 x10^{-6} cm^3 mol^{-1} compared to DCM with a molar susceptibility of -46.6 x10^{-6} cm^3 mol^{-1} [52]. Hence if the previous assumption was incorrect, diamagnetic repulsion of the solute would be reduced through the use of a CTC mobile phase. The force experienced by a diamagnetic solute for each conformation with a CTC and DCM mobile phase are presented in Table 3. Calculation using Equation 10 predicts over an 85% increase in diamagnetic force experienced by the iodine solute in a DCM mobile phase compared to CTC.

Table 3: Diamagnetic force experienced by an iodine solute calculated using Equation 10 for a CTC and a DCM mobile phase.

Orientation	**Diamagnetic force in CTC mobile phase /N mol^{-1}**	**Diamagnetic force in DCM mobile phase /N mol^{-1}**
Alternating	1.0 ×10^{-3}	1.9 ×10^{-3}
Repeating	2.2 ×10^{-4}	4.2 ×10^{-4}
Rotating	8.0 ×10^{-4}	1.5 ×10^{-3}

3.4.5 Solute migration using a dichloromethane mobile phase in the presence of magnetic fields

With the change in mobile phase, implications for the system regarding the transparency of the stationary phase had to also be considered. Unexpectedly, the translucent nature of the column remained unchanged to the eye, and still permitted the transmission of light through the column to the detector. This allowed the data analysis and the on-column visualisation system to remain unchanged for solute migration analysis using the DCM mobile phase.

The 4.0 mm column was repacked for analysis using the DCM mobile phase. Band morphology appeared similar to the 4.0 mm column prepared for solute migration in the CTC mobile phase presented in Figure 25. This meant that, as with the previous analysis, the entire solute profile was unable to be imaged. That is, part of the peak tail was not able to be measured. Duplicate performance checks were performed both before and after all analysis was completed to evaluate if changes in peak shape or solute distribution occurred over the time period. The peak shapes at the outmost radial band (-0.9), which was located near the magnet arrays is presented in Figure 28. Note the tailing portion of the band which was not imaged.

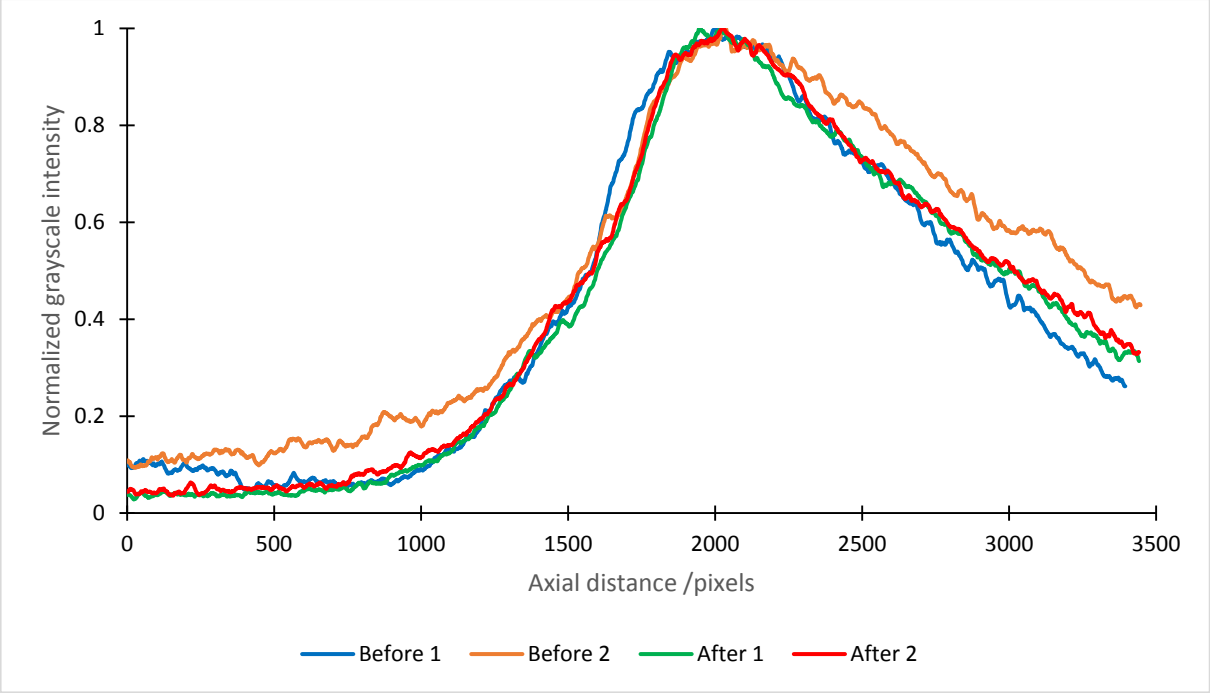

Figure 28: Performance check showing the peak profiles measured at a normalized radius of -0.9 for a 10 µL injection of 12 g L^{-1} iodine in DCM solution after 1.5 minutes. Duplicate runs were performed before (blue and orange) and after (green and red) solute migration runs were performed.

No degradation of column performance appeared to occur over the period of the analysis as peak shape remained consistent to a good degree for injections performed before and after

analysis. All measured peaks were broad in shape with a significant tailing component that was unable to be imaged in its entirety. Small inconsistencies were observed however, for the second duplicate performed before analysis. The peak from this injection was broader in shape compared to other injections. Overall, the performance check indicated that peaks shape at a normalized radius of -0.9 was reproducible to an acceptable degree and may be used as an indicator for diamagnetic repulsion for injections run between the performance checks.

The solute distribution of the duplicate runs was also determined before and after the analysis sequence to analyse if any drift occurred in this respect. The distribution of iodine across the 4.0 mm ID column is presented in Figure 29. Excellent agreement between the injections was determined for the solute distribution across the column diameter. The distribution was relatively symmetrical, with a slightly higher loading on the left hand side of the column. Small differences were observed for the first duplicate performed before analysis (blue) on the right hand side of the column where a lower grayscale intensity was measured. Overall, iodine distribution on the left side of the column was shown highly reproducible.

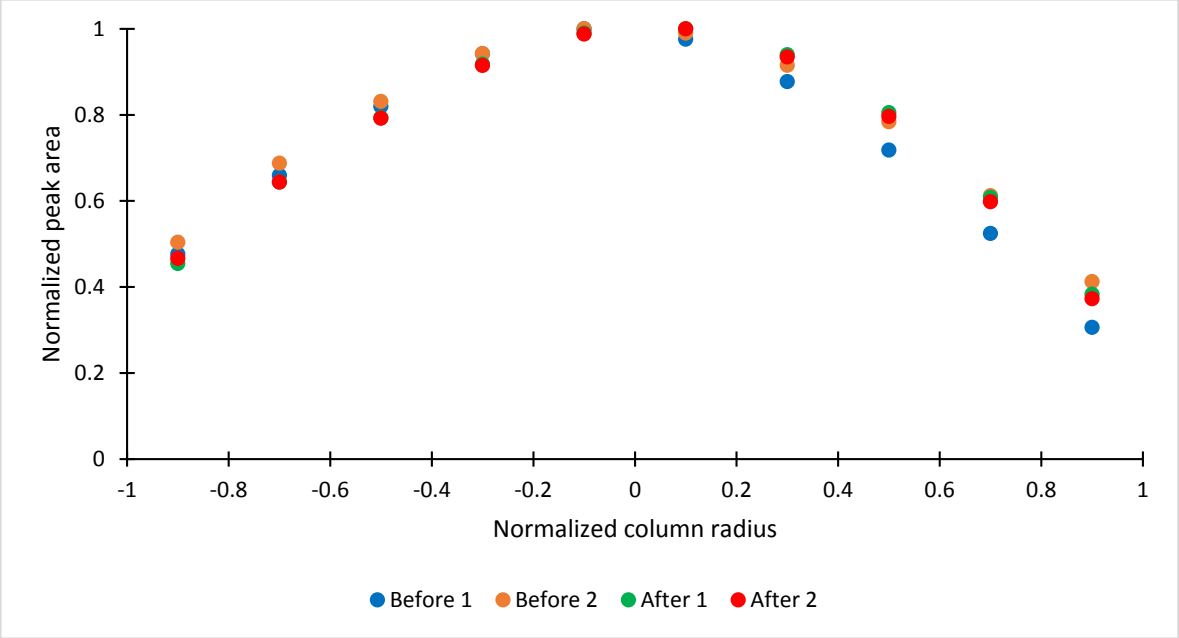

Figure 29: Performance check showing the normalized solute distribution of iodine across the diameter of a 4.0 mm ID column after 1.5 minutes. Distributions are shown for duplicate 10 µL injections of 12 g L^{-1} iodine in DCM performed before (blue and orange) and after (green and red) solute migration analysis runs.

Triplicate 10 µL injections of 12 g L^{-1} iodine in DCM were analysed in the absence of magnets and the presence of an alternating, repeating and rotating magnet conformation array. Peak shapes for the radial location of -0.9 (closest the magnet assembly) was averaged for the triplicates

and compared in Figure 30. Under each condition, the shape of the radial peak remained constant. Small variations were observed to the tailing portion of the band but no significant changes that may be indicative of diamagnetic repulsion. This result was confirmed by the solute distribution presented in in Figure 31, where the distribution of iodine across the 4.0 mm diameter for each conformation remained within the experimental uncertainty.

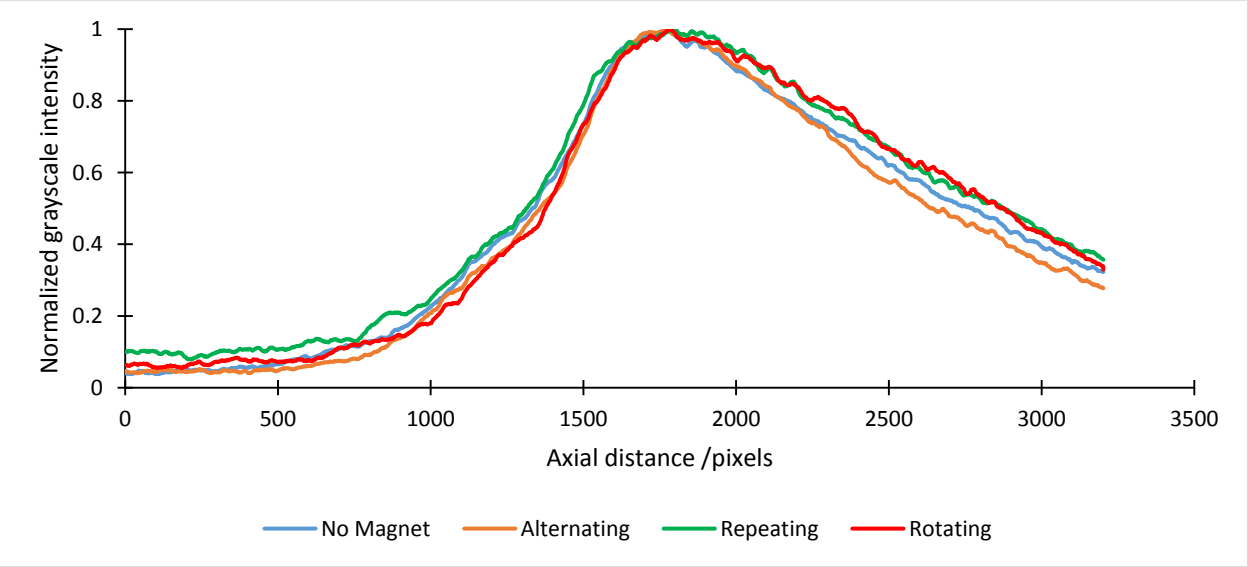

Figure 30: Average peak shapes for triplicate 10 µL injections of 12 g L^{-1} iodine in DCM after 1.5 minutes. Injections were performed in the absence of magnetic fields (blue) and in the presence of alternating (orange), repeating (green) and rotating (red) magnet assemblies.

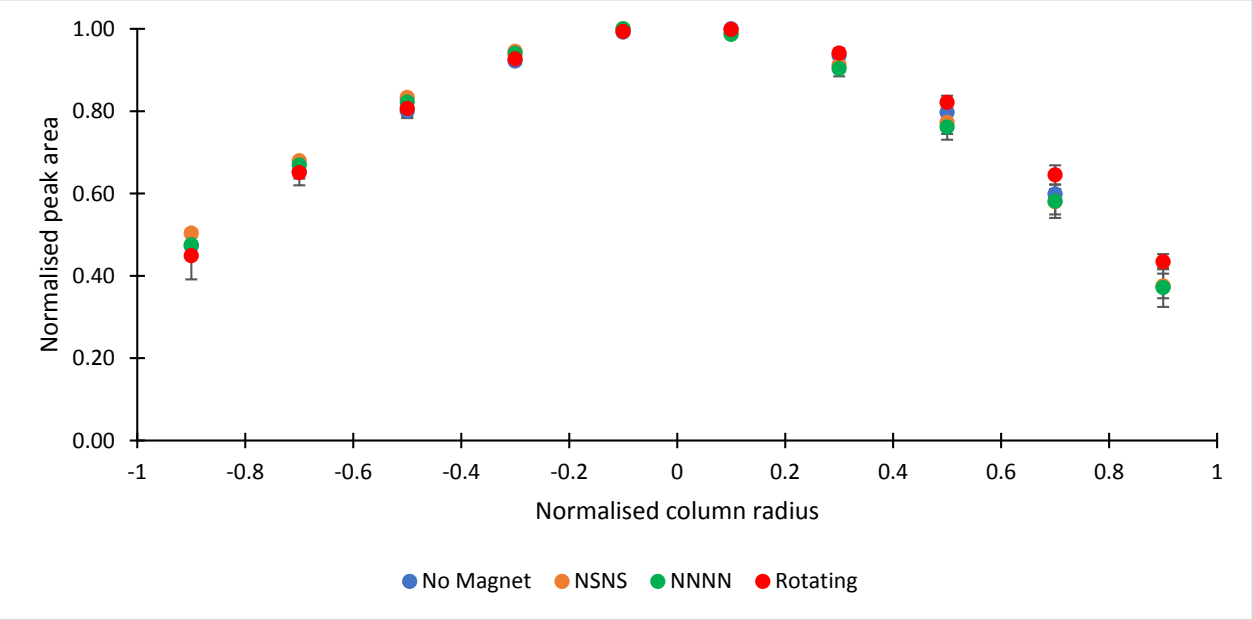

Figure 31: Normalized solute distribution of a 10 µL injection of 12 g L^{-1} iodine in DCM across the diameter of a 4.0 mm ID column after 1.5 minutes. Distribution was calculated for elution in the absence of magnetic fields (blue) and in the presence of a alternating (orange), repeating (green) and rotating (red) conformation. Data points represent the average of the triplicate analysis and error bars representing the standard deviation of the triplicate injections.

Despite the chromatography system mimicking the conditions of the proof of principle experiments, solute migration was unable to be observed. Stationary phase type, solute and mobile phase were all replicated in the final solute migration experiment. Column dimensions were also matched as closely possible. This indicates that positioning of the magnet arrays may have not been ideal for the purposes of diamagnetic repulsion. Positioning of the magnets in the proof of principle experiment was achieved using freehand or by crude means with both positive and negative results being recorded. The initial response to this indication that magnet position was important was the development of the magnet apparatus. However, its limitation was that its design only enabled column arrays to be investigated with the chromatography column positioned at the arrays centre. This positioning is illustrated in Figure 32 with simulated flux lines. The FEMM simulation suggests that the central positioning of the column relative to the array may have not been ideal. If accurate, the results from each experiment would be expected to produce a negative result as they did. Shifting the position of the column to the edge or side of the magnet array may be more favourable for producing a measurable effect.

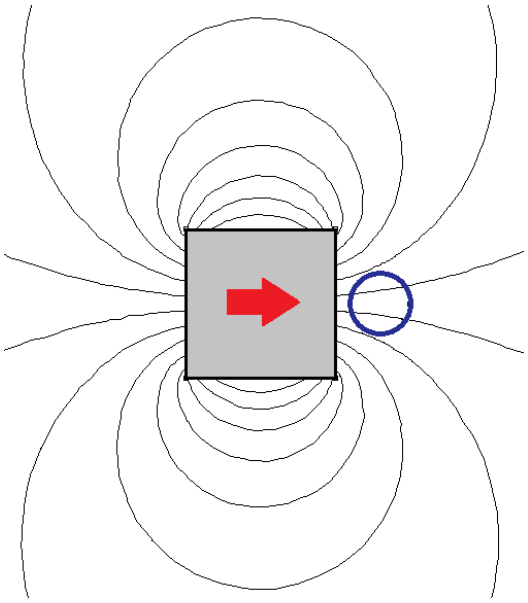

Figure 32: FEMM simulation of magnetic flux contours of a 10 mm × 10 mm neodymium magnet. Magnetised direction is indicated with the red arrow. The blue circle indicates location of the 4.0 mm ID column at a distance of 1 mm from the magnet surface.

3.5 Future Directions

The future direction for this research must be first to reproduce the diamagnetic repulsion achieved in the proof of principle experiments on a chromatography system that allows on-column visualisation. This must involve the development and investigation of new magnet arrays that incorporate different column positioning relative to the array. To inform this future direction of research, more advanced modelling of magnetic environments will be required to optimise the magnetic flux and flux gradients experienced by the column. This may be achieved using 3-dimensional simulations to address the limitations of 2-dimensional simulation highlighted in this study.

Once repulsion is optimized, a magnetic apparatus can be applied to a standard HPLC analysis to determine whether an increase in efficiency or a favourable change in peak shape is achieved. If successful, the applicability of diamagnetic repulsion may be investigated through the trial of various mobile phases, analytes, stationary phases, column dimensions and other parameters.

Chapter 4: Conclusion

This study consisted of three major aims including: (a) demonstrating diamagnetic repulsion had the potential to manipulate solute migration in a chromatography column through a proof of principle experiment, (b) development of a liquid chromatography system that allowed the on-column visualisation of solute migration and (c) quantifying the effects of various magnetic environments on solute migration in a chromatography column.

A proof of principle experiment was successfully performed through the positioning of neodymium magnets against the wall of small scale pipette columns. A distinct migration of the iodine solute from the magnet surface was observed indicating diamagnetic repulsion as a possible means to mediate the wall effects. The positive result prompted investigation into the effect using a more controlled system.

The construction of an on-column visualisation chromatography was subsequently achieved using the principles of matched refractive indices. A borosilicate column was packed with a silica stationary phase and a CTC mobile phase passed through. This allowed visualisation of an iodine solute for the duration of its elution. Determination of solute profiles and distributions throughout the column using the system was found to be highly reproducible for replicate injections using both 15 mm and 4.0 mm ID column formats.

The effects of various magnetic environments on solute migration in the column was also successfully achieved. A total of three magnetic orientations were trialled in three distinct conditions; a 15 mm ID column with a CTC mobile phase, a 4.0 mm ID column with a CTC mobile phase and a 4.0 mm ID column with a DCM mobile phase. In each instance, a negative result was obtained with no detectable migration of the iodine solute away from the magnet array. Peak shape was also found to remain unchanged in the presence of magnetic fields for both the 15 mm and 4.0 mm ID formats. The disagreement between the proof of concept experiment and solute migration analysis using the developed chromatography system may have been a result of non-optimal positioning of permanent magnets.

Future research should be directed towards reproducing the diamagnetic repulsion achieved in the proof of principle experiment on a system that permits on-column visualisation. This may be achieved through the development and 3-dimensional simulation of new magnet arrays and positioning that maximises the magnetic flux and flux gradients experienced by the column.

Reference List

(1) Van Deemter, J. J.; Zuiderweg, F.; Klinkenberg, A. v. *Chemical Engineering Science* **1956**, *5*, 271.
(2) Cielecka-Piontek, J.; Zalewski, P.; Jelińska, A.; Garbacki, P. *Chromatographia* **2013**, *76*, 1429.
(3) Knox, J. H.; Parcher, J. F. *Analytical Chemistry* **1969**, *41*, 1599.
(4) Knox, J. H.; Laird, G. R.; Raven, P. A. *Journal of Chromatography A* **1976**, *122*, 129.
(5) Gritti, F.; Guiochon, G. *Analytical chemistry* **2013**, *85*, 3017.
(6) Shalliker, R. A.; Broyles, B. S.; Guiochon, G. *Journal of Chromatography A* **2000**, *888*, 1.
(7) Shalliker, R. A.; Ritchie, H. *Journal of Chromatography A* **2014**, *1335*, 122.
(8) Khirevich, S.; Höltzel, A.; Seidel-Morgenstern, A.; Tallarek, U. *Journal of Chromatography A* **2012**, *1262*, 77.
(9) Bruns, S.; Stoeckel, D.; Smarsly, B. M.; Tallarek, U. *Journal of Chromatography A* **2012**, *1268*, 53.
(10) Broeckhoven, K.; Desmet, G. *Journal of Chromatography A* **2007**, *1172*, 25.
(11) Khirevich, S.; Höltzel, A.; Seidel-Morgenstern, A.; Tallarek, U. *Analytical chemistry* **2009**, *81*, 7057.
(12) Guiochon, G.; Farkas, T.; Guan-Sajonz, H.; Koh, J.-H.; Sarker, M.; Stanley, B. J.; Yun, T. *Journal of Chromatography A* **1997**, *762*, 83.
(13) Shalliker, R. A.; Wong, V.; Broyles, B. S.; Guiochon, G. *Journal of Chromatography A* **2002**, *977*, 213.
(14) Yew, B. G.; Drumm, E. C.; Guiochon, G. *AIChE journal* **2003**, *49*, 626.
(15) Guiochon, G.; Drumm, E.; Cherrak, D. *Journal of Chromatography A* **1999**, *835*, 41.
(16) Yew, B. G.; Ureta, J.; Shalliker, R. A.; Drumm, E. C.; Guiochon, G. *AIChE journal* **2003**, *49*, 642.
(17) Farkas, T.; Sepaniak, M. J.; Guiochon, G. *Journal of Chromatography A* **1996**, *740*, 169.
(18) Tallarek, U.; Bayer, E.; Van Dusschoten, D.; Scheenen, T.; Van As, H.; Guiochon, G.; Neue, U. D. *AIChE journal* **1998**, *44*, 1962.
(19) Mriziq, K. S.; Abia, J. A.; Lee, Y.; Guiochon, G. *Journal of Chromatography A* **2008**, *1193*, 97.
(20) Abia, J. A.; Mriziq, K. S.; Guiochon, G. A. *Journal of Chromatography A* **2009**, *1216*, 3185.
(21) Gritti, F.; Guiochon, G. *Journal of Chromatography A* **2012**, *1225*, 79.
(22) Baur, J. E.; Wightman, R. M. *Journal of Chromatography A* **1989**, *482*, 65.
(23) Farkas, T.; Chambers, J. Q.; Guiochon, G. *Journal of Chromatography A* **1994**, *679*, 231.
(24) Farkas, T.; Guiochon, G. *Analytical Chemistry* **1997**, *69*, 4592.
(25) Farkas, T.; Sepaniak, M. J.; Guiochon, G. *AIChE journal* **1997**, *43*, 1964.
(26) Bayer, E.; Müller, W.; Ilg, M.; Albert, K. *Angewandte Chemie International Edition in English* **1989**, *28*, 1029.
(27) Fernandez, E. J.; Grotegut, C. A.; Braun, G. W.; Kirschner, K. J.; Staudaher, J. R.; Dickson, M. L.; Fernandez, V. L. *Physics of Fluids (1994-present)* **1995**, *7*, 468.
(28) Park, J. C.; Raghavan, K.; Gibbs, S. J. *Journal of Chromatography A* **2002**, *945*, 65.
(29) Shalliker, R. A.; Broyles, B. S.; Guiochon, G. *Journal of Chromatography A* **1998**, *826*, 1.
(30) Shalliker, R. A.; Broyles, B. S.; Guiochon, G. *Analytical chemistry* **2000**, *72*, 323.
(31) Bruns, S.; Müllner, T.; Kollmann, M.; Schachtner, J.; Höltzel, A.; Tallarek, U. *Analytical chemistry* **2010**, *82*, 6569.
(32) Hlushkou, D.; Bruns, S.; Höltzel, A.; Tallarek, U. *Analytical chemistry* **2010**, *82*, 7150.

(33) Hormann, K.; Müllner, T.; Bruns, S.; Höltzel, A.; Tallarek, U. *Journal of Chromatography A* **2012**, *1222*, 46.
(34) Bruns, S.; Grinias, J. P.; Blue, L. E.; Jorgenson, J. W.; Tallarek, U. *Analytical chemistry* **2012**, *84*, 4496.
(35) Bruns, S.; Franklin, E. G.; Grinias, J. P.; Godinho, J. M.; Jorgenson, J. W.; Tallarek, U. *Journal of Chromatography A* **2013**, *1318*, 189.
(36) Ritchie, H.; Shalliker, R. A.; Google Patents: 2012.
(37) Camenzuli, M.; Ritchie, H. J.; Ladine, J. R.; Shalliker, R. A. *Journal of Chromatography A* **2012**, *1232*, 47.
(38) Camenzuli, M.; Ritchie, H. J.; Ladine, J. R.; Shalliker, R. A. *Analyst* **2011**, *136*, 5127.
(39) Shalliker, R.; Camenzuli, M.; Pereira, L.; Ritchie, H. *Journal of Chromatography A* **2012**, *1262*, 64.
(40) Gritti, F.; Guiochon, G. *Journal of Chromatography A* **2013**, *1297*, 64.
(41) Foley, D.; Pereira, L.; Camenzuli, M.; Edge, T.; Ritchie, H.; Shalliker, R. *Microchemical Journal* **2013**, *110*, 127.
(42) Bain, G. A.; Berry, J. F. *Journal of Chemical Education* **2008**, *85*, 532.
(43) Earnshaw, A. *Introduction to magnetochemistry*; Elsevier, 2013.
(44) Watarai, H.; Namba, M. *Journal of chromatography A* **2002**, *961*, 3.
(45) Shen, F.; Hwang, H.; Hahn, Y. K.; Park, J.-K. *Analytical chemistry* **2012**, *84*, 3075.
(46) Winkleman, A.; Perez-Castillejos, R.; Gudiksen, K. L.; Phillips, S. T.; Prentiss, M.; Whitesides, G. M. *Analytical chemistry* **2007**, *79*, 6542.
(47) Tarn, M. D.; Hirota, N.; Iles, A.; Pamme, N. *Science and Technology of Advanced Materials* **2009**, *10*, 014611.
(48) Peyman, S. A.; Kwan, E. Y.; Margarson, O.; Iles, A.; Pamme, N. *Journal of Chromatography A* **2009**, *1216*, 9055.
(49) Winkleman, A.; Gudiksen, K. L.; Ryan, D.; Whitesides, G. M.; Greenfield, D.; Prentiss, M. *Applied physics letters* **2004**, *85*, 2411.
(50) Rodríguez-Villarreal, A. I.; Tarn, M. D.; Madden, L. A.; Lutz, J. B.; Greenman, J.; Samitier, J.; Pamme, N. *Lab on a Chip* **2011**, *11*, 1240.
(51) Rowland, R. S.; Taylor, R. *The Journal of Physical Chemistry* **1996**, *100*, 7384.
(52) Lide, D. R. *CRC Handbook of chemistry and physics* **2000**, *86*, 130.